Some general features of mesophase formation in hard-core potentials

D. Pini[1,*]

[1] *Dipartimento di Fisica "A. Pontremoli", Università degli Studi di Milano, Via Celoria 16, 20133 Milano, Italy*

Abstract

The formation of mesophases in fluids with hard-core plus tail interactions is investigated and compared with the occurrence of cluster crystals in ultra-soft repulsive potentials by using a simple variational expression for the Helmholtz free energy. The purpose of this study is mostly qualitative, i.e., to explain the origin of the different behavior of these systems, and the reason why, in the hard-core case, interactions which are apparently quite different display a common pattern for the phase diagram, featuring clusters, bars, lamellae, inverted bars, and inverted clusters as the density is increased. In the limit of zero temperature, our approach also yields some simple predictions for the densities at which the transitions between different mesophases are expected to take place, as well as for the size of their aggregates at the transitions. We find that these results compare favorably with those obtained in a former study of a model fluid with competing attractive and repulsive interactions by density-functional theory with numerical minimization.

* davide.pini@fisica.unimi.it

I. INTRODUCTION

Spontaneous self-assembly into ordered structures is a fascinating property of soft matter and an example of how, when collective properties are considered, even simple models can lead to a surprisingly rich behavior. A relevant case in this respect is represented by ultra-soft repulsive potentials [1, 2], which may be thought of as a representation of the effective interactions between branched macromolecules such as dendrimers [3]. Another instance is that of compact, hard-core particles whose potential features, besides the hard-sphere contribution, a short-range attractive and long-range repulsive (SALR) tail [4–20], due e.g. to the combination of depletion and screened electrostatic effective forces. In terms of the interactions between their constituents, the physical explanation of the mechanism leading to self-assembly is quite different in the two systems. In the former case, clustering occurs because, due to the very soft character of the repulsion, above a certain density strong overlap between the relatively few particles within each cluster is energetically favored with respect to partial overlap between many particles [21]. In the latter case, instead, clusters are formed because of the competition between the attraction, which favors particle aggregation, and the repulsion, which prevents the coalescence of clusters and the transition into two macroscopic liquid and vapor phases.

Nevertheless, in both instances the attitude to self-assembly rests upon the same property of the Fourier transform of the pair potential (or, for hard-core particles, of its non-singular part), namely, the fact that it takes its absolute minimum at a non-vanishing wave vector k_0. This favors the spontaneous occurrence of density modulations with characteristic length $\lambda \sim 2\pi/k_0$ which, under suitable thermodynamic conditions, can lead to genuinely periodic inhomogeneous phases. For soft repulsive interactions, potentials of this kind are said to belong to the $Q^{\pm}$ class [22].

However, this does not imply that soft- and hard-core interactions which share such a property have the same kind of phase portrait. In fact, while ultra-soft $Q^{\pm}$ potentials are predicted to form only crystals of strongly localized, globular clusters [2], hard-core SALR potentials display a more complex behavior. Specifically, on increasing the density one goes through a sequence featuring globular cluster, tubular, lamellar as well as inverted-tubular and inverted-cluster mesophases, in which the particle-rich and particle-depleted regions are switched with respect to their "direct" counterpart. Moreover, bicontinuous phases are

observed in two domains nested between the tubular and lamellar or lamellar and inverted-tubular phases.

This pattern has emerged many times in a number of theoretical studies based on coarse-grained [11–15, 20] or microscopic [18, 19] free-energy functionals, and also in recent numerical simulations [16]. In fact, it had been uncovered before in a different system where frustration inhibits a macroscopic phase separation, namely, block copolymer melts [23, 24]. For fluids of unconnected particles such as those considered here, it is not even peculiar to the SALR potential, but is found more generally provided the hard core is followed by an interaction featuring the minimum at $k_0 \neq 0$ in Fourier space, such as a soft repulsive shoulder [12, 25, 26].

The fact that these fluids can be described in terms of a common coarse-grained effective functional [12] already provides an explanation for their similar phase behavior. But what is the physical mechanism leading to it? The purpose of this paper is to contribute to answer this question by providing a simple explanation of the general aspects of mesophase formation in hard-core fluids: specifically, what is the origin of the sequence clusters/bars/lamellae/inverted bars/inverted clusters found for increasing density in systems with different tail interactions, and why this behavior differs from that of soft-core $Q^{\pm}$ potentials.

Accordingly, our treatment will be mostly qualitative and rely on a simple variational expression of the free energy similar to that developed in Ref. [2] for soft-core potentials, in which the features specific to the interaction are conveyed into a small number of parameters. Because of the simplified character of the description, we shall not be considering bicontinuous phases such as the gyroid which, albeit interesting, are generally found only in a narrow domain of the phase diagram [12, 16, 19], similarly to block copolymers [24].

We also find that, in the limit of vanishing temperature, our approach easily yields some predictions for the densities at which the transitions between different mesophases take place, as well as for the size of the globular, tubular, or lamellar domains at the transitions. We have tested these predictions against the results which we had obtained for a specific SALR interaction in a former study [19] based on the numerical minimization of the full free-energy functional, and found a rather satisfactory agreement, especially considering the approximate character of the present treatment.

The paper is organized as follows: in Section II we describe the method which we have

adopted, starting from a mean-field density functional for the Helmholtz free energy and introducing additional approximations. In Section III the application to soft-core $Q^{\pm}$ potentials is considered. The results basically reproduce those obtained in Ref. [2] for this kind of interactions, but we thought it useful to include them in order to keep the presentation self-contained. Hard-core interactions are addressed in Sections IV and V, which deal with direct and inverted phases respectively. The limits of the present approximate treatment are discussed in Section VI, together with a comparison between the threshold temperatures of the various mesophases determined here and the results of a recent simulation study [16]. In Section VII the behavior of the theory at zero temperature is illustrated, and the values of the densities and sizes of the various phases at the transitions are obtained. The comparison between the predicted sizes and those determined in Ref. [19] for a specific SALR potential at finite temperature is performed in Section VIII. Finally, in Section IX we summarize our findings and draw our conclusions.

II. ANALYTICAL APPROXIMATION

We shall be considering a fluid of particles interacting via a spherically symmetric pair potential which consists of a hard core and a non-singular tail $w(r)$ whose Fourier transform assumes its negative minimum at a wave vector $k_0 \neq 0$, and shall compare its phase behavior with that of an ultra-soft $Q^{\pm}$ potential. Even though we are clearly abusing the term since the Fourier transform of $w(r)$ does not necessarily have to change sign, hereafter we shall refer to such a hard-core fluid as hard-core $Q^{\pm}$ for convenience.

In order to describe the regular structures formed by these systems, we shall start from a simple density functional for the Helmholtz free energy F which has already been employed a number of times to this purpose in both the soft- [1, 2] and hard-core case [10, 19]. The contribution to F due to $w(r)$ is described in the mean-field approximation:

$$\beta F = \int d^3\mathbf{r}\, \rho(\mathbf{r}) f_{\rm ref}[\rho(\mathbf{r})] + \frac{\beta}{2} \int d^3\mathbf{r} \int d^3\mathbf{r}'\, \rho(\mathbf{r})\rho(\mathbf{r}')w(\mathbf{r}-\mathbf{r}')\,, \tag{1}$$

where $f_{\rm ref}(\rho)$ is the Helmholtz free energy per particle and unit temperature of the unperturbed or "reference" fluid such that $w(r) \equiv 0$, $\rho(\mathbf{r})$ is the density profile, and $\beta = 1/k_{\rm B}T$, $k_{\rm B}$ being the Boltzmann constant. For a hard-core fluid, the reference term of Eq. (1) is also approximate, and for $f_{\rm ref}$ the standard Carnahan-Starling expression [27] has been used in

this study. For a soft-core interaction, instead, $w(r)$ coincides with the full potential, and $f_{\rm ref}(\rho)$ with the corresponding quantity for the ideal gas, which is exactly described by the reference term of Eq. (1).

If $\rho(\mathbf{r})$ is periodic, Eq. (1) can be rewritten as

$$\frac{\beta F}{V} = \frac{1}{v}\int_v d^3\mathbf{r}\,\rho(\mathbf{r}) f_{\rm ref}[\rho(\mathbf{r})] + \frac{\beta}{2v^2}\sum_{\mathbf{k}} \hat{\rho}_{\mathbf{k}}\hat{\rho}_{-\mathbf{k}}\widetilde{w}(\mathbf{k})\,, \tag{2}$$

where v is the volume of a primitive cell of the Bravais lattice, and the sum runs over the sites of the reciprocal lattice. The Fourier integral $\hat{\rho}_{\mathbf{k}}$ of the density profile is performed over the volume of the primitive cell:

$$\hat{\rho}_{\mathbf{k}} = \int_v d^3\mathbf{r}\, e^{i\mathbf{k}\cdot\mathbf{r}}\rho(\mathbf{r})\,, \tag{3}$$

while the Fourier transform $\widetilde{w}(\mathbf{k})$ of the interaction, which is not a periodic function, is performed over the whole space. Let us assume that the density profile can be represented by a sum of characteristic functions centered at the lattice sites $\mathbf{R}$:

$$\rho(\mathbf{r}) = \bar{\rho}\sum_{\mathbf{R}} \chi(\mathbf{r}-\mathbf{R})\,. \tag{4}$$

Here, $\chi(\mathbf{r})$ denotes the characteristic function of a domain which we take as a sphere (S), a cylinder (C), or a lamella (L):

$$\chi_{\rm S}(\mathbf{r}) = \begin{cases} 1 & |\mathbf{r}| < \gamma\,, \\ 0 & |\mathbf{r}| > \gamma\,. \end{cases} \tag{5}$$

$$\chi_{\rm C}(\mathbf{r}) = \begin{cases} 1 & |\mathbf{r}_\perp| < \gamma\,, \\ 0 & |\mathbf{r}_\perp| > \gamma\,. \end{cases} \tag{6}$$

$$\chi_{\rm L}(\mathbf{r}) = \begin{cases} 1 & |r_\parallel| < \gamma\,, \\ 0 & |r_\parallel| > \gamma\,, \end{cases} \tag{7}$$

where $\mathbf{r}_\perp$ and $r_\parallel$ are respectively the transverse and longitudinal components of $\mathbf{r}$, and γ is the radius of the sphere for $\chi_{\rm S}$, the radius of the cylinder for $\chi_{\rm C}$, and the half-width of the lamella for $\chi_{\rm L}$.

Strictly speaking, the above assumption is quantitatively justified only in the strong-segregation regime at low temperatures, when $\rho(\mathbf{r})$ does have a sharp interface which separates very populated and nearly empty domains, and the mesophases can then be regarded

as made by compact "objects" with a well-defined shape. Within this description, the most accurate way to proceed would consist in determining the interaction between such objects by integrating *a la* Hamaker $w(\mathbf{r})$ over their volume. However, our main task here is not so much quantitative accuracy, as to give a simple picture of the general features of mesophase formation in hard-core fluids, and we feel that the expressions thus obtained do not lend themselves well to this purpose, because they are involved, and may mask the underlying mechanism, instead of bringing it out. Accordingly, we shall rely on a different strategy based on Eq. (2), along the lines put forth in Ref. [2] for soft-core interactions.

Let us first consider the density $\bar{\rho}$ inside an aggregate: this is related to the average density $\rho = \int d^3\mathbf{r}\, \rho(\mathbf{r})/V$ by

$$\bar{\rho}_{\mathrm{S}} = \frac{3\,\rho v}{4\pi\gamma^3}\,, \tag{8}$$

$$\bar{\rho}_{\mathrm{C}} = \frac{\rho s}{\pi\gamma^2}\,, \tag{9}$$

$$\bar{\rho}_{\mathrm{L}} = \frac{\rho l}{2\gamma}\,, \tag{10}$$

for spheres, cylinders, and lamellae respectively. Here, s is the surface of the primitive cell of the two-dimensional lattice formed by cylinders, and l is the length of the primitive cell of the one-dimensional lattice formed by lamellae. If we use Eqs. (4), (5)–(7) and (8)–(10) in Eq. (2) we obtain for the free energy per particle

$$\frac{\beta F}{N} = f_{\mathrm{ref}}(\bar{\rho}) + \frac{\beta\rho}{2}\sum_{\mathbf{k}} \widetilde{w}(\mathbf{k})\varphi(\gamma k)\,, \tag{11}$$

where the form factor φ is a positive, monotonically decreasing function of its dimensionless argument λ such that $\varphi(0) = 1$, whose expression depends on whether one is considering spheres, cylinders, or lamellae. Specifically, we have:

$$\varphi_{\mathrm{S}}(\lambda) = \left[\, \frac{3}{\lambda^3}\,(\sin\lambda - \lambda\cos\lambda)\,\right]^2\,, \tag{12}$$

$$\varphi_{\mathrm{C}}(\lambda) = \left[\, 2\,\frac{J_1(\lambda)}{\lambda}\,\right]^2\,, \tag{13}$$

$$\varphi_{\mathrm{L}}(\lambda) = \left[\, \frac{\sin\lambda}{\lambda}\,\right]^2\,, \tag{14}$$

where $J_1(\lambda)$ is the Bessel function of order 1. If Eq. (4) is to represent a localized arrangement of spheres, cylinders or lamellae, the size of the aggregates γ and the nearest-neighbor distance a must satisfy the relation

$$2\gamma < a\,. \tag{15}$$

Moreover, a can be expressed as

$$a = \frac{\theta}{\kappa}\,, \tag{16}$$

where κ is the nearest-neighbor distance of the reciprocal lattice and θ is a lattice-dependent constant which is given by

$$\theta_{\rm bcc} = \sqrt{6}\pi\,, \tag{17}$$

$$\theta_{\rm triang} = \frac{4\sqrt{3}\pi}{3}\,, \tag{18}$$

$$\theta_{\rm 1d} = 2\pi\,, \tag{19}$$

for the bcc, two-dimensional triangular and one-dimensional lattices respectively. Here the bcc and triangular lattices have been considered instead of other possibilities such as the simple cubic, the fcc, the hcp, or the square lattices because, according to the present treatment, they correspond to the most stable configurations in three and two dimensions, as will be discussed in the following.

Equations (15) and (16) lead to

$$\gamma\kappa < \theta/2\,. \tag{20}$$

From now on, we shall set $\lambda = \gamma\kappa$. Figure 1 displays the functions $\varphi_{\rm S}$, $\varphi_{\rm C}$, $\varphi_{\rm L}$ in the interval $0 < \lambda < \theta/2$. One has $\varphi_{\rm L}(\lambda) < \varphi_{\rm C}(\lambda) < \varphi_{\rm S}(\lambda)$ over the whole interval communal to their domains.

Let us now turn to Eqs. (8)–(10) for $\bar{\rho}$. These expressions contain the size of the primitive cell, which can be written as ζa^d, where d is the dimension of the lattice and ζ is a lattice-dependent constant. If a is subsequently expressed as function of κ via Eqs. (17)–(19), we obtain

$$\bar{\rho} = \frac{\alpha\rho}{\lambda^d}\,, \tag{21}$$

where α is a lattice-dependent constant given by

$$\alpha_{\rm bcc} = 6\sqrt{2}\pi^2 \simeq 83.7\,, \tag{22}$$

$$\alpha_{\rm triang} = \frac{8\sqrt{3}\pi}{3} \simeq 14.5\,, \tag{23}$$

$$\alpha_{\rm 1d} = \pi \simeq 3.14\,. \tag{24}$$

We observe that α increases considerably on increasing d. As will be discussed in the following, this property plays a key role in determining the sequence of mesophases commonly observed in hard-core fluids.

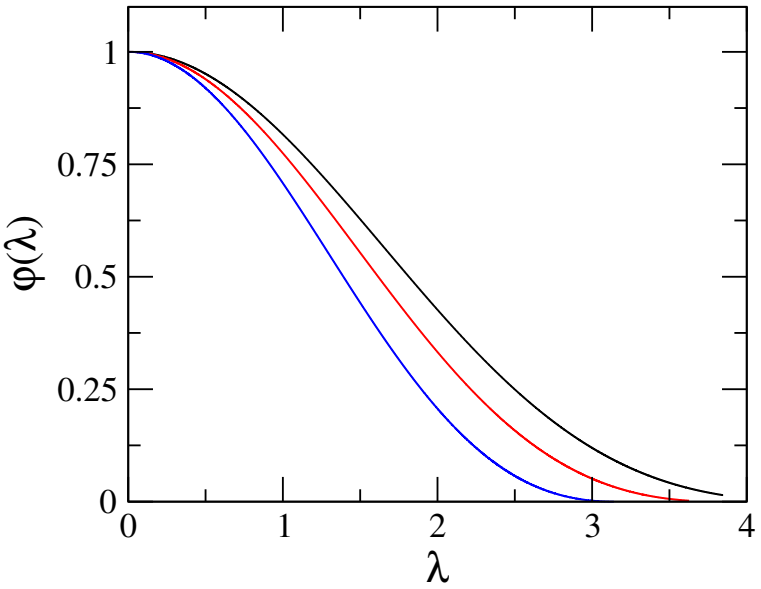

FIG. 1. Form factors $\varphi(\lambda)$ of Eqs. (12)–(14) as a function of the dimensionless domain size $\lambda = \gamma\kappa$ for spheres (black line), cylinders (red line), and lamellae (blue line).

By substituting Eq. (21) in Eq. (11) and taking into account that the argument of the sum over $\mathbf{k}$ is spherically symmetric, Eq. (11) can be rewritten as

$$\frac{\beta F}{N} = f_{\rm ref}\left(\frac{\alpha\rho}{\lambda^d}\right) + \frac{\beta\rho}{2}\widetilde{w}(0) + \frac{\beta\rho}{2}\sum_{i=1}^{\infty} n_i \widetilde{w}(\nu_i\kappa)\varphi(\nu_i\lambda)\,, \tag{25}$$

where the sum is carried out over all neighbor shells in the reciprocal space, n_i is the coordination number of shell i, and ν_i are lattice-dependent constants expressing the radius of shell i in terms of the nearest-neighbor distance κ. Clearly, one has $\nu_1 = 1$. We must now look for the minimum of Eq. (25) as a function of the lattice spacing a and the aggregate size γ at fixed ρ and β. Since the relation between (a, γ) and (κ, λ) is invertible, we can switch to κ, λ as independent variables, and minimize Eq. (25) with respect to them. By differentiating Eq. (25) with respect to κ and λ we find straightforwardly

$$\sum_{i=1}^{\infty} n_i\nu_i\widetilde{w}\,'(\nu_i\kappa)\varphi(\nu_i\lambda) = 0\,, \tag{26}$$

$$-\frac{d}{\lambda}Z_{\rm ref}\left(\frac{\alpha\rho}{\lambda^d}\right) + \frac{\beta\rho}{2}\sum_{i=1}^{\infty} n_i\nu_i\widetilde{w}(\nu_i\kappa)\varphi'(\nu_i\lambda) = 0\,, \tag{27}$$

where $Z_{\rm ref}$ is the compressibility factor of the reference system and the primes denote the derivatives of the functions $\widetilde{w}(k)$ and $\varphi(\lambda)$.

From now on, we shall make the approximation of truncating the sum in Eqs. (25)–(27) to the nearest-neighbor shell in reciprocal space, following Ref. [2] for soft-core $Q^{\pm}$ potentials. That is not to say that Fourier components beyond nearest neighbors are not there, as this would be inconsistent with Eqs. (5)–(7), but rather that the first shell accounts for the largest part of the free energy due to the off-core part of the interaction. We are aware that such an assumption is questionable and shall come back to it in Section VI. Nevertheless, even though we shall admittedly give up accuracy for simplicity sake, we are willing to do so as long as this allows a qualitative picture of the phase behavior and of the role played by the different contributions to the free energy.

Equation (25) becomes then

$$\frac{\beta\Delta F}{N} = f_{\rm ref}\left(\frac{\alpha\rho}{\lambda^d}\right) - f_{\rm ref}(\rho) + \frac{\beta\rho}{2} q\widetilde{w}(\kappa)\varphi(\lambda)\,, \tag{28}$$

where we have introduced the difference ΔF between the Helmholtz free energy of the inhomogeneous phase and that of the homogeneous phase at the same temperature and density in the mean-field approximation. The latter is obtained by setting $\rho(\mathbf{r}) \equiv \rho$ in Eq. (1).

Conditions (26) and (27) become

$$\widetilde{w}\,'(\kappa)\varphi(\lambda) = 0\,, \tag{29}$$

$$-\frac{d}{\lambda} Z_{\rm ref}\left(\frac{\alpha\rho}{\lambda^d}\right) + \frac{\beta\rho}{2} q\widetilde{w}(\kappa)\varphi'(\lambda) = 0\,, \tag{30}$$

where $q \equiv n_1$ is the number of nearest neighbors of the reciprocal lattice. We observe that $\varphi(\lambda)$ vanishes only for the lamellar phase at $\lambda = \pi$, which corresponds to the homogeneous phase such that $\gamma = a/2$. Hence, according to Eq. (29) an inhomogeneous phase must necessarily satisfy $\widetilde{w}\,'(\kappa) = 0$. The root at $\kappa = 0$ can be ruled out, since it would give $\lambda = 0$ and therefore a divergence of $\bar{\rho}$. One has then to look for roots at $\kappa \neq 0$, if they exist. If this is the case, then Eq. (28) shows that the lowest free energy corresponds to $\kappa = k_0$, where k_0 is the wave vector at which $\widetilde{w}(k)$ reaches its absolute minimum. Therefore, in the present one-shell approximation, the lattice constant is a state-independent quantity intrinsic to $w(r)$, as already discussed in Ref. [2] for soft $Q^{\pm}$ interactions. Since Eq. (29) is the same irrespective of the reference system, the same conclusion holds also for the hard-core plus tail potentials considered here, although it should be pointed out that this hinges on the approximate description of the hard-sphere reference system given by functional (1). What

determines the different behavior between hard- and soft-core fluids is Eq. (30) for λ, as will be discussed in the following.

III. SOFT-CORE $Q^{\pm}$ POTENTIALS

It is first instructive to consider the case of soft-core potentials studied in Refs. [1, 2]. In fact, for this class of interactions the choice of Eq. (4) to parametrize $\rho(\mathbf{r})$ is rather artificial, since in those works it was shown that $\rho(\mathbf{r})$ is described almost exactly by a superposition of Gaussians. Nevertheless, we shall stick to Eq. (4) because, as stated above, here we are mainly interested in the qualitative features of the phase diagram, and would like to compare the soft- and hard-core cases on as much an equal footing as possible. In this respect, Eq. (4), though not particularly accurate, can be considered as the roughest example of a density profile which includes an amplitude $\bar{\rho}$ and a width γ.

For soft-core potentials, the reference system coincides with the ideal gas and we have $f_{\rm ref}(\rho) = \ln\rho - 1$, $Z_{\rm ref} = 1$. The discussion then follows closely that of Ref. [2]. Equations (28) and (30) become

$$\frac{\beta\Delta F}{N} = \ln\left(\frac{\alpha}{\lambda^d}\right) - \frac{q w_0}{2}\beta\rho\varphi(\lambda)\,, \tag{31}$$

$$-\frac{q}{2d}\lambda\,\varphi'(\lambda) = \frac{1}{w_0\beta\rho}\,, \tag{32}$$

where we have set $w_0 \equiv |\widetilde{w}(k_0)|$. The graphical solution of Eq. (32) for spheres, cylinders and lamellae is displayed in Fig. (2). When a solution exists, the smaller root corresponds to a minimum of the free energy, while the larger root corresponds to a maximum. We observe that, since $\varphi_{\rm S}(\lambda)$, $\varphi_{\rm C}(\lambda)$ and $\varphi_{\rm L}(\lambda)$ are similar, the largest value of the l.h.s. of Eq. (32) for a given λ pertains to the phase with the largest ratio q/d between the coordination number q of the reciprocal lattice and the dimensionality d of the modulation. Hence, if one moves from the homogeneous domain, the bcc cluster phase with $q/d = 4$ is met for smaller values of $\beta\rho$ than the triangular tubular phase with $q/d = 3$, which in turn is met for smaller $\beta\rho$ than the lamellar phase with $q/d = 2$.

Moreover, even when $\beta\rho$ is large enough to allow also for tubular or both tubular and lamellar phases, the cluster phase is always that which has the largest q and the smallest λ at a given thermodynamic state. Both of these features go in the direction of making the excess term in Eq. (31) more negative, thus leading to a lower free energy. It might be

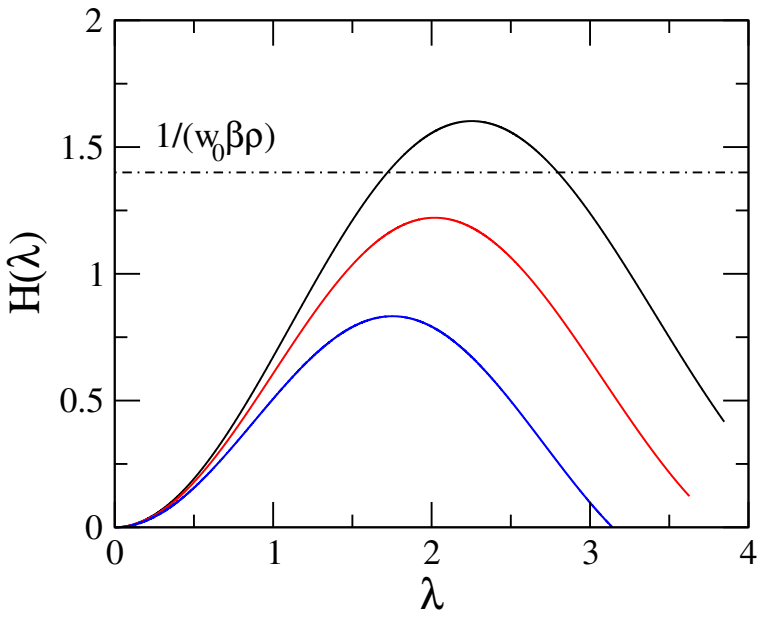

FIG. 2. Graphical solution of Eq. (32) for the dimensionless domain size λ. $H(\lambda)$ is the l.h.s. of Eq. (32) for spheres (black line), cylinders (red line), and lamellae (blue line). The solution at given β and ρ is the smaller λ at which $H(\lambda)$ intersects the dash-dotted line.

argued that the effect on the reference part in Eq. (31) goes in the opposite direction, since the cluster phase also has the largest α and the largest d, which gives the largest cluster density $\bar{\rho}$ and the largest $f_{\rm ref}(\bar{\rho})$. However, the weak logarithmic dependence on $\bar{\rho}$ of the ideal-gas $f_{\rm ref}$ is not sufficient to contrast the decrease of the excess contribution. This is made evident by substituting Eq. (32) in Eq. (31) to obtain

$$\frac{\beta\Delta F}{N} = \ln\left(\frac{\alpha}{\lambda^d}\right) + \frac{d\,\varphi(\lambda)}{\lambda\varphi'(\lambda)}\,, \tag{33}$$

As pointed out in Ref. [2], the density and temperature appear in Eq. (33) only via λ and hence only via the combination $\beta\rho$. When λ is varied, Eqs. (32) and (33) give the free energy as a function of density and temperature in parametric form.

Figure 2 shows that, as $\beta\rho$ increases, the solution of Eq. (32) which corresponds to a minimum of the free energy gets smaller and smaller, i.e., particles become more and more localized. At small λ, the divergence of the logarithmic term in Eq. (33) is swamped by the power-law divergence of the (negative) excess contribution. The latter behaves as $-A/\lambda^2$, with $A_{\rm S} = 15/2$, $A_{\rm C} = 4$, $A_{\rm L} = 3/2$ for spheres, cylinders, and lamellae respectively. Hence,

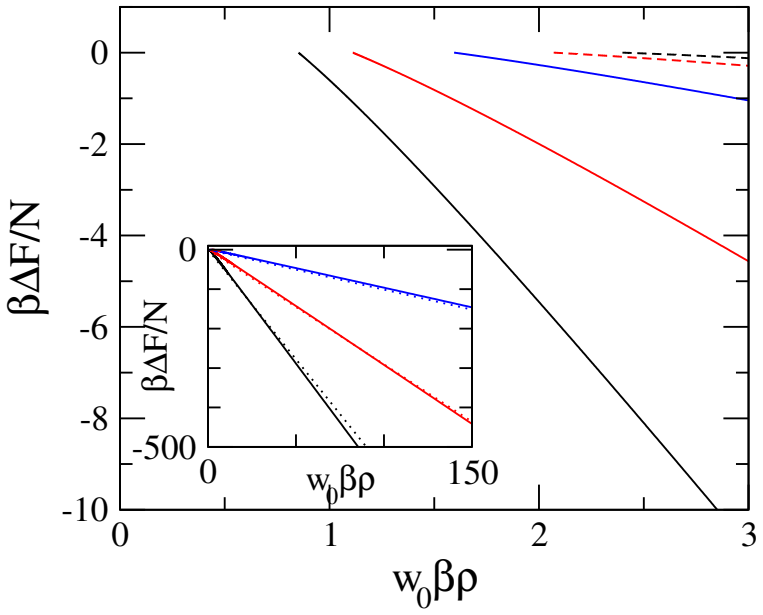

FIG. 3. Difference ΔF between the reduced Helmholtz free energy of the inhomogeneous phase and that of the homogeneous fluid for spheres (solid black line), cylinders (solid red line), lamellae (solid blue line), inverted cylinders (dashed red line), and inverted spheres (dashed black line) for soft-core $Q^{\pm}$ fluids. Only the region of negative ΔF has been displayed. The inset shows ΔF at large $\beta\rho$ for spheres, cylinders, and lamellae compared with $\beta\rho S/2$, where S is the lattice sum of Eq. (55) over the bcc (black dotted line), triangular (red dotted line), and one-dimensional (blue dotted line) reciprocal lattices for the GEM-4 potential $w(r) = \exp[-(r/\sigma)^4]$, see Section VI.

for large values of $\beta\rho$ the excess term dominates and Eq. (31) becomes simply

$$\frac{\beta\Delta F}{N} \underset{\beta\rho\gg 1}{\sim} -\frac{qw_0}{2}\beta\rho\,. \tag{34}$$

Figure 3 displays ΔF as a function of $\beta\rho$ for spheres, cylinders, and lamellae. For each phase, ΔF is indeed a monotonically decreasing, nearly linear function of $\beta\rho$ such that the lowest ΔF always pertains to the phase with the largest q. Therefore, spherical clusters always win over cylinders and lamellae. The request that ΔF be negative in order for the cluster phase to be stable with respect to the homogeneous fluid leads to $\lambda < \lambda_0 \simeq 1.461$. The melting line at which ΔF vanishes is obtained by estimating Eq. (32) at $\lambda = \lambda_0$ and is given by $1/(\beta\rho) = 1.173w_0$, to be compared with the (more accurate) result $1/(\beta\rho) = 1.393w_0$ obtained in Ref. [2] by representing $\rho(\mathbf{r})$ as a sum of Gaussians.

To summarize: for soft-core $Q^{\pm}$ potentials such that particle overlap is allowed, regular

arrangements of aggregates of many particles are always favored with respect to the homogeneous phase below a threshold value of T/ρ. As T/ρ decreases, the size of the aggregates γ *decreases indefinitely*, while their density *increases indefinitely* according to Eq. (21). Finally, according to the one-shell approximation (31), the bcc crystal of spherical aggregates is always preferred to either a two-dimensional crystal of bars or a one-dimensional crystal of lamellae, owing to the larger number of neighbors q of its reciprocal lattice.

IV. HARD-CORE $Q^{\pm}$ POTENTIALS

The scenario described above changes completely as one moves from soft- to hard-core potentials. In this case, both $f_{\rm ref}(\rho)$ and $Z_{\rm ref}(\rho)$ diverge at finite ρ. According to the Carnahan-Starling equation used here, one has

$$f_{\rm ref}(\rho) = \ln\rho - 1 + \frac{\eta(4-3\eta)}{(1-\eta)^2}\,, \tag{35}$$

$$Z_{\rm ref}(\rho) = \frac{1+\eta+\eta^2-\eta^3}{(1-\eta)^3}\,, \tag{36}$$

where $\eta = \pi\rho\sigma^3/6$ is the packing fraction, σ being the hard-sphere diameter. In fact, the true upper limit for η is set by the value at close packing, so that the density $\bar{\rho}$ inside a domain cannot exceed $\rho_{\rm cp} = \sqrt{2}/\sigma^3$. In the following, density and temperature will be measured in reduced units such that

$$\rho^* \equiv \rho\sigma^3\,, \tag{37}$$

$$T^* \equiv \frac{k_{\rm B}T\sigma^3}{w_0} \tag{38}$$

For a given average density ρ, Eq. (21) gives a lower bound on λ:

$$\lambda > \left(\frac{\alpha\rho^*}{\sqrt{2}}\right)^{1/d}\,, \tag{39}$$

If this condition is combined with the upper bound on λ given by Eq. (20) which forbids overlap between neighboring aggregates, one obtains an upper bound $\rho^*_{\rm B}$ on ρ^* for the existence of a given mesophase. In particular, one has

$$\rho^* < \rho^*_{\rm B,\,bcc} = \frac{\sqrt{6}\pi}{8} \simeq 0.96\,, \tag{40}$$

$$\rho^* < \rho^*_{\rm B,\,triang} = \frac{\sqrt{6}\pi}{6} \simeq 1.28\,, \tag{41}$$

$$\rho^* < \rho^*_{\rm B,\,1d} = \sqrt{2} \simeq 1.41 \tag{42}$$

for the bcc, triangular, and lamellar phase respectively. For the lamellar phase, $\rho_{\rm B}^*$ coincides with $\rho_{\rm cp}^*$ because it is possible to obtain a close-packed arrangement of spheres over the whole space by taking a close-packed arrangement of spheres over each stripe, and having the stripes coalesce so as to fill the space. For tubular and cluster phases, the analogous process would always leave empty gaps between neighboring aggregates, so that $\bar{\rho}$ reaches the value at close packing before ρ does. This, however, says nothing about the relative stability of these phases at the densities at which all of them are allowed, such as those we are interested in.

Let us then turn to Eq. (30) with $Z_{\rm ref}(\rho)$ given by Eq. (36). In order to solve this equation over the ρ-axis at fixed β, we may express ρ in terms of $\bar{\rho}$ via Eq. (21) to get

$$-\frac{q\lambda^{d+1}}{2\alpha d}\varphi'(\lambda) = \frac{Z_{\rm ref}(\bar{\rho})}{w_0\beta\bar{\rho}}\,. \tag{43}$$

For each phase, Eq. (43) is solved with respect to $\bar{\rho}$. An example of the solution procedure is sketched in Fig. 4 for $T^* = 0.022$. For a given λ, the r.h.s. of Eq. (43) is read from Fig.4(a), and the corresponding value of $Z_{\rm ref}(\bar{\rho})/\bar{\rho}$ is obtained. The densities $\bar{\rho}$ are then found from Fig. 4(b), and the average density ρ is determined from λ and $\bar{\rho}$ via Eq. (21). The values of $\bar{\rho}$ and ρ are then inserted into Eq. (28) for the free energy. As λ varies in the interval $0 < \lambda < \theta/2$, one gets the free energy as a function of ρ in parametric form.

Unlike in the soft-core case considered in the previous Section, the r.h.s. of Eq. (43) now depends separately on β and ρ instead of being a function of the single variable $\beta\rho$, and the same applies to the quantity $\beta\Delta F/N$. In particular, it is clear from Fig. 4 that there is a temperature above which no solution to Eq. (43) is found irrespective of the density. This is due to the fact that in Eq. (43) the l.h.s. has a maximum as a function of λ, while the r.h.s. has a minimum as a function of $\bar{\rho}$. As a consequence, for Eq. (43) to have solutions at all, it is necessary that β satisfies the condition

$$\frac{1}{w_0\beta}\frac{Z_{\rm ref}(\bar{\rho}_{\rm m})}{\bar{\rho}_{\rm m}} \leq -\frac{q}{2\alpha d}\lambda_{\rm M}^{d+1}\varphi'(\lambda_{\rm M})\,, \tag{44}$$

where $\bar{\rho}_{\rm m}$ and $\lambda_{\rm M}$ are the values of $\bar{\rho}$ and λ at which the r.h.s. and l.h.s. of Eq. (43) assume respectively their minimum and maximum. Since the largest maximum of the l.h.s. of Eq. (43) pertains to the lamellae, the lamellar phase is the first to appear as the temperature is lowered, to be followed by the bar triangular and the cluster bcc phases. However, the requirement that Eq. (43) admits solutions is only a necessary condition for the occurrence

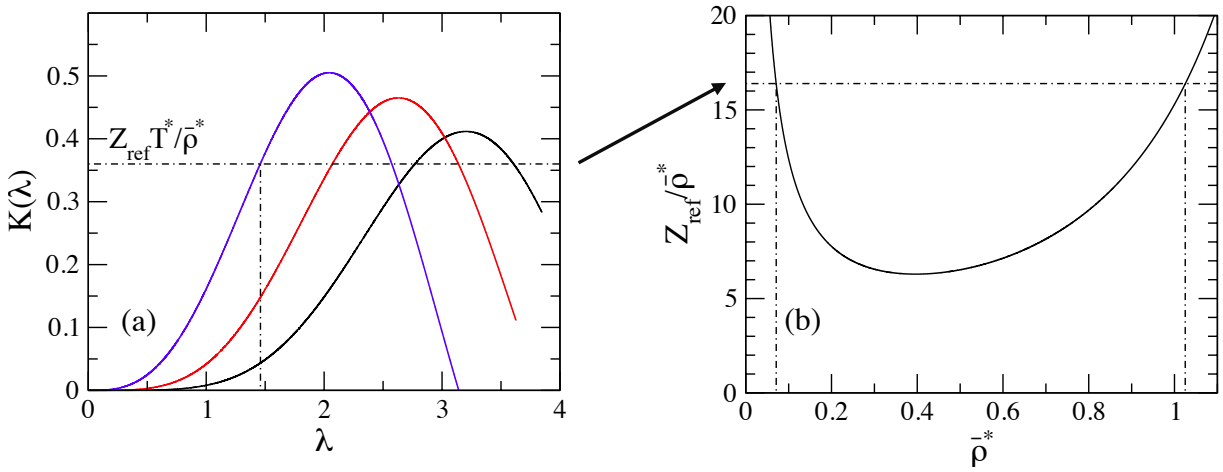

FIG. 4. Graphical solution of Eq. (43). In panel (a), $K(\lambda)$ is the l.h.s. of Eq. (43) for spheres (black line), cylinders (red line), and lamellae (blue line). For a given reduced temperature T^* (here, $T^* = 0.022$), $K(\lambda)$ yields $Z_{\rm ref}(\bar{\rho})/\bar{\rho}$. The solutions at given λ and T^* are obtained by the values of $\bar{\rho}$ at which the solid curve in panel (b) intersects the horizontal dash-dotted line. The corresponding values of ρ are then obtained by Eq. (21).

of a given phase. In order for that phase to be actually stable, it is also required that its ΔF be negative and larger in absolute value than those of the other phases at the same density, if they exist. This leads to the following maximum allowed temperatures $T_{\rm max}$ for each of the phases in hand:

$$T^*_{\rm max,\,bcc} = 0.0439, \quad T^*_{\rm max,\,triang} = 0.0569, \quad T^*_{\rm max,\,1d} = 0.0629\,. \tag{45}$$

These values can be compared with the temperature on the top of the so-called λ-line. This is defined as the boundary of the domain of the T-ρ plane inside which the homogeneous phase becomes thermodynamically unstable against the formation of mesophases, and is then akin to the spinodal line for the liquid-vapor transition. According to functional (1), the λ-line is given by

$$\frac{1}{w_0\beta} = \rho\,\chi^{\rm R}_{\rm ref}(\rho)\,, \tag{46}$$

where $\chi^{\rm R}_{\rm ref}(\rho)$ is the reduced isothermal compressibility of the reference hard-sphere fluid obtained from Eq. (36). The temperature along the λ-line reaches its maximum at $\rho^*_\lambda = 0.249$, $T^*_\lambda = 0.0901$, so that, even for the lamellar phase, $T^*_{\rm max}$ is significantly lower than T^*_λ. The reason for such a discrepancy is that, according to the mean-field functional (1) on which Eq. (28) for ΔF is based, at the top of the λ-line the transition from the inhomogeneous to

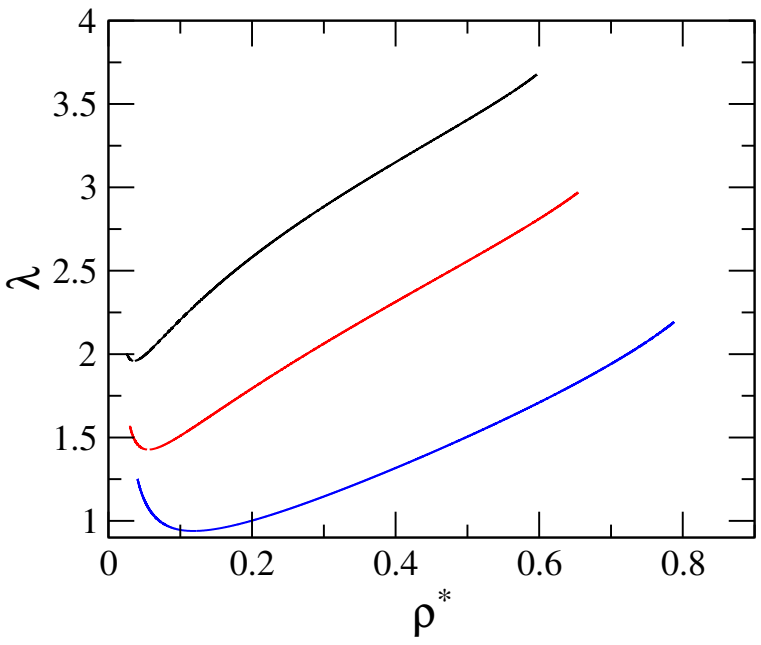

FIG. 5. Dimensionless size $\lambda = \gamma\kappa$ of spheres (black line), cylinders (red line), and lamellae (blue line) according to Eq. (43) for hard-core $Q^{\pm}$ fluids at $T^* = 0.022$ as a function of the reduced density. Only the region of negative ΔF has been displayed.

the homogeneous fluid is second-order, i.e., the amplitude of the density modulation tends to zero as one approaches T_λ. This behavior cannot be represented by the density profile of Eq. (4), in which the amplitude jumps discontinuously from $\bar{\rho}$ to 0. As observed above, this parameterization is justifed only at low temperatures. Near the top of the λ-line, a treatment in which $\rho(\mathbf{r})$ is regarded as a perturbation superimposed to a uniform density is definitely more adequate [11, 13].

At temperatures such that Eq. (43) admits solutions, we see from panel (b) that a given value of $Z_{\rm ref}(\bar{\rho})/\bar{\rho}$ corresponds to two values of $\bar{\rho}$, and hence to two values of ρ. Moreover, the l.h.s. of Eq. (43) is a non-monotonic function of λ so that, as λ is changed, a part or even the whole interval of allowed values of $\bar{\rho}$ may be spanned twice. As a consequence, a part or even the whole interval of the resulting values of ρ may be obtained for two different λ and hence two different $\bar{\rho}$, resulting in two branches for λ and ΔF as a function of ρ. Clearly, in such an instance the branch which gives the lower ΔF is chosen.

The results thus obtained for λ and ΔF as a function of ρ are displayed in Figs. 5 and 6 for $T^* = 0.022$. Except for a narrow interval at small ρ, now λ *increases* with ρ, at variance with soft-core fluids. Moreover, for each phase, either bcc, triangular, or lamellar, ΔF is not

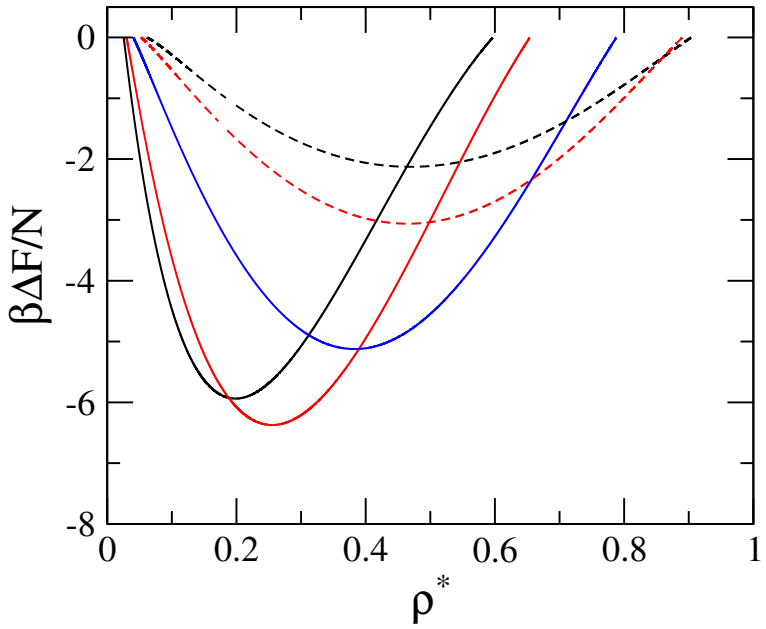

FIG. 6. Difference ΔF between the Helmholtz free energy of the inhomogeneous phase and that of the homogeneous fluid for spheres (solid black line), cylinders (solid red line), lamellae (solid blue line), inverted cylinders (dashed red line), and inverted spheres (dashed black line) for hard-core $Q^{\pm}$ fluids at $T^* = 0.022$. Only the region of negative ΔF has been displayed.

a monotonically decreasing function of ρ anymore, but has instead a minimum at a certain ρ. The reason for this behavior is the strong divergence of $f_{\rm ref}(\rho)$ of Eq. (35) at high density: according to Eq. (21), having λ decrease as ρ increases would lead to a rapid increase of $\bar{\rho}$ and hence to the uncontrolled growth of $f_{\rm ref}(\bar{\rho})$ in Eq. (28). To prevent this unfavorable situation, λ *must* increase with ρ so as to keep $\bar{\rho}$ well below close packing, except possibly at very small ρ such that $\bar{\rho}$ would still remain small even on decreasing λ. This state of affairs has an important consequence: while for soft-core fluids increasing ρ also leads to an increase of $\varphi(\lambda)$ (recall that $\varphi(\lambda)$ is a monotonically decreasing function of λ), and thus to a decrease of the (negative) interaction contribution to the free energy in Eq. (28), now ρ and $\varphi(\lambda)$ have competing effects on this contribution. At first, as ρ increases it is ρ itself which prevails. However, ρ cannot increase indefinitely, while at the upper bound for λ given by Eq. (20), $\varphi(\lambda)$ vanishes (for lamellae) or nearly so (for spheres and cylinders). As a consequence, $\varphi(\lambda)$ eventually wins and the free energy starts to increase, thereby assuming a minimum as a function of ρ.

The same mechanism lies at the heart of the different phase behavior of hard- and soft-

core fluids: as shown again in Fig. 6, as the density is increased at fixed temperature, the most stable phase changes from spheres to cylinders to lamellae, at variance with the behavior depicted in Fig. 3. As in the soft-core case, as far as the coordination number q is concerned, lamellae are unfavored compared to cylinders, which are in turn unfavored compared to spheres. However, now one has to take into account also the aforementioned decrease of $\varphi(\lambda)$ on increasing ρ, which tends to increase the free energy by making its off-core contribution less negative. The key point is that the coefficient α in Eq. (21) decreases substantially when the dimension d of the aggregates decreases, see Eqs. (22)–(24). As a consequence, decreasing d at fixed ρ allows one to keep the hard-sphere contribution to the free energy at bay by obtaining a similar, or possibly even smaller $\bar{\rho}$ *at the price of a significantly smaller* λ. Although one has $\varphi_{\rm L}(\lambda) < \varphi_{\rm C}(\lambda) < \varphi_{\rm S}(\lambda)$ for *the same* λ, these functions are similar to one another, so that one obtains a larger $\varphi(\lambda)$ for the phase at lower d, provided the decrease in λ is substantial. At high enough ρ, the ensuing gain in the off-core part of the free energy more than compensates for the loss due to the lower q, and the phase with the lower dimension takes over. At the transition, there is a considerable decrease in λ, and hence in the size γ of the mesophase domains, as pointed out in Ref. [19].

Therefore, the sequence clusters/bars/lamellae as the density is increased emerges as the result of the competition between the preference for large values of q, which favors high d, and the preference for phases which pack more efficiently, which favors low d. For soft-core potentials the latter requirement is not an issue, and high-d cluster phases are always favored.

The above considerations rest on the dependence of λ on ρ at fixed T. The dependence of λ on T at fixed ρ is best elucidated by turning back from Eq. (43) to Eq. (30) and casting it into the form

$$-\frac{q}{2d}\,\frac{\lambda\,\varphi'(\lambda)}{Z_{\rm ref}(\alpha\rho/\lambda^d)} = \frac{1}{w_0\beta\rho}\,. \tag{47}$$

By comparing Eq. (47) with Eq. (32) one sees immediately that the l.h.s. of Eq. (47) vanishes at the lower bound of λ at which $Z_{\rm ref}$ diverges, and initially increases on increasing λ. The graphical solution of Eq. (47) at fixed ρ is then similar to that of Eq. (32) shown in Fig. 2: the λ which minimizes the free energy is located in the increasing region, while the root in the decreasing region, if it exists, corresponds to a maximum. When the temperature is decreased, the r.h.s. of Eq. (47) decreases, and hence λ must also decrease. Figure 7 displays

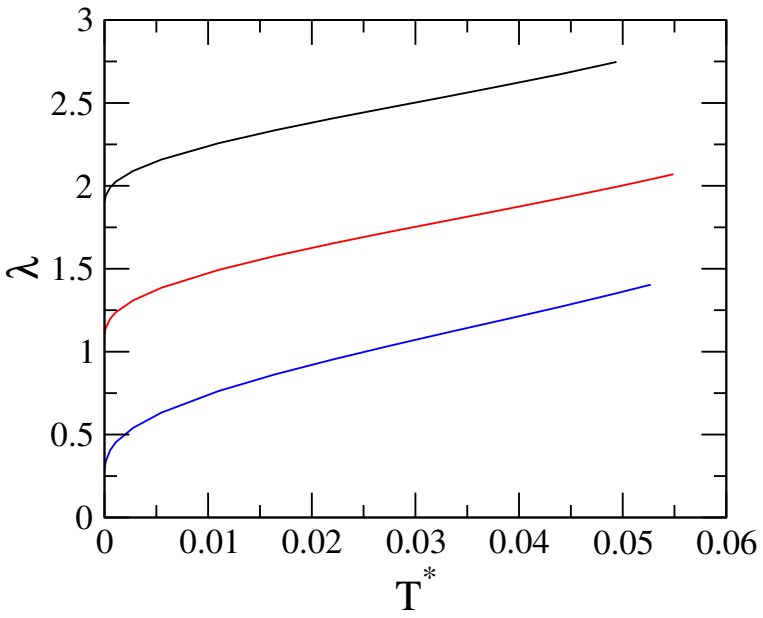

FIG. 7. Dimensionless size $\lambda = \gamma\kappa$ of spheres (black line), cylinders (red line), and lamellae (blue line) according to Eq. (43) for hard-core $Q^{\pm}$ fluids at $\rho^* = 0.15$ as a function of the reduced temperature. Only the region of negative ΔF has been displayed.

λ as a function of T^* at fixed density $\rho^* = 0.15$ for clusters, bars, and lamellae. While λ as a function of ρ behaves very differently for soft- and hard-core interactions, the behavior as a function of T is qualitatively similar, inasmuch as λ is an increasing function of T in both cases. However, in soft-core systems λ vanishes for $T \to 0$. This never happens in hard-core systems, where the lower bound of λ is dictated by the condition $\bar{\rho} < \rho_{\rm cp}$. The behavior in the limit $T \to 0$ will be discussed in Section VII.

V. INVERTED PHASES

Considerations similar to those developed in the previous Section explain another important feature of the phase behavior of hard-core $Q^{\pm}$ potentials which is not found in soft-core systems, namely, the occurrence at high density of inverted cluster and inverted cylinder phases. In these phases the spherical or columnar domains are basically empty, and the particles are distributed in the remaining space, so that they can be obtained from those already considered by exchanging the filled and empty regions. Within the present treatment

this is done straightforwardly by replacing the density profile of Eq. (4) by

$$\rho(\mathbf{r}) = \bar{\rho}\,[\,1 - \sum_{\mathbf{R}} \chi(\mathbf{r} - \mathbf{R})\,]\,, \tag{48}$$

where $\bar{\rho}$ now represents the density outside the empty holes. Equation (21) is then replaced by

$$\bar{\rho} = \frac{\alpha\rho}{\alpha - \lambda^d}\,. \tag{49}$$

By performing the Fourier integral of $\rho(\mathbf{r})$, substituting in into Eq. (2) and truncating the sum over the reciprocal lattice vectors to the nearest-neighbor shell as before, we obtain instead of Eq. (28)

$$\frac{\beta\Delta F}{N} = f_{\rm ref}\left(\frac{\alpha\rho}{\alpha - \lambda^d}\right) - f_{\rm ref}(\rho) + \frac{\beta\rho}{2} q\widetilde{w}(\kappa)\psi(\lambda)\,, \tag{50}$$

where we have set

$$\psi(\lambda) = \left(\frac{\lambda^d}{\alpha - \lambda^d}\right)^2 \varphi(\lambda)\,. \tag{51}$$

We observe that the free energy of the inverted-lamellar phase is mapped into that of the lamellar phase under the transformation $\lambda \to \pi - \lambda$ as one would expect, since for lamellae a phase with empty regions of size λ is identical to a phase with filled regions of size $\pi - \lambda$.

By minimizing the above expression for the free energy with respect to κ, one finds again that κ has to coincide with the wave vector k_0 of the absolute minimum of $\widetilde{w}(k)$. The minimization with respect to λ gives

$$\frac{q\lambda^{d+1}}{2\alpha d}\left(\frac{\alpha}{\lambda^d} - 1\right)^2 \psi'(\lambda) = \frac{Z_{\rm ref}(\bar{\rho})}{w_0\beta\bar{\rho}}\,, \tag{52}$$

which replaces Eq. (43).

For soft-core interactions such that $f_{\rm ref}(\rho) = \ln\rho - 1$, $Z_{\rm ref} = 1$, Eqs. (32) and (33) are replaced by

$$\frac{q}{2d}\,\frac{\alpha - \lambda^d}{\lambda^{d-1}}\psi'(\lambda) = \frac{1}{w_0\beta\rho}\,, \tag{53}$$

$$\frac{\beta\Delta F}{N} = \ln\left(\frac{\alpha}{\alpha - \lambda^d}\right) - \frac{d\lambda^{d-1}}{\alpha - \lambda^d}\,\frac{\psi(\lambda)}{\psi'(\lambda)}\,, \tag{54}$$

where the minimum of the free energy at given $\beta\rho$ corresponds to the larger root of Eq. (53). It is found that, at variance with the solution of Eq. (32) for "direct" phases, here λ increases on increasing $\beta\rho$. However, since in this case λ represents the size of the holes, the effect is that as $\beta\rho$ is increased, particles are squeezed into a smaller region for both direct and

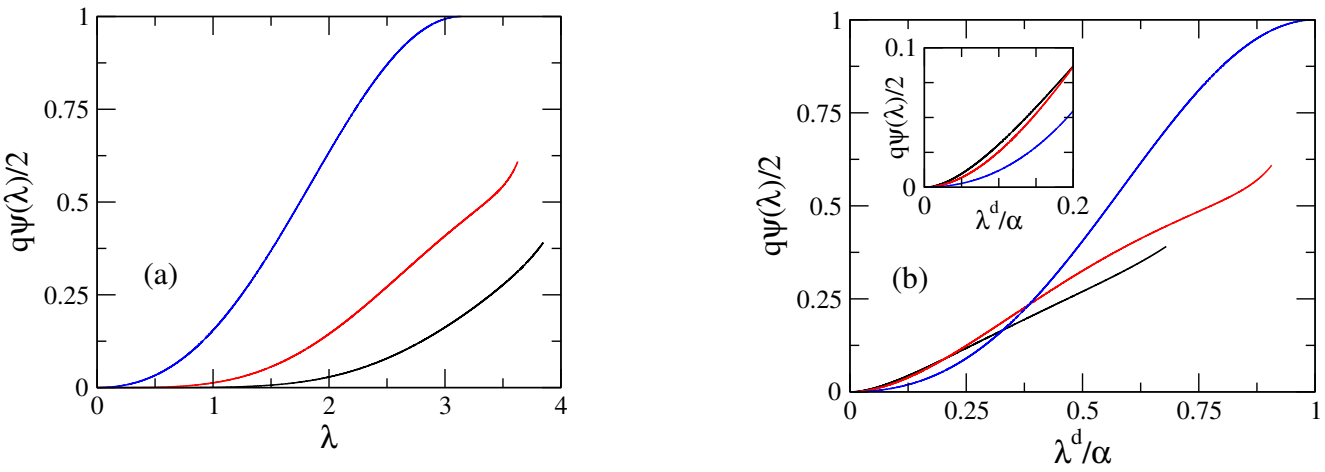

FIG. 8. Panel (a): quantity $q\psi(\lambda)/2$ for spheres (black line), cylinders (red line), and lamellae (blue line) as a function of λ, where $\psi(\lambda)$ is the form factor of the inverted phases defined in Eq. (51) and $\lambda = \gamma\kappa$ is the dimensionless size of the spherical, cylindrical, or lamellar holes. Panel (b): same quantity as a function of λ^d/α, where α is the lattice-dependent constant of Eqs. (22)–(24). The inset is a magnification of the region at small λ.

inverted phases. In fact, the present representation of the inverted phases is valid provided the density is not so high, that λ exceeds the upper limit set by Eq. (20).

In Fig. 3 the free energies of the inverted cluster and inverted cylinder phases have been plotted together with those of the direct phases discussed before. Although the inverted phases are favored with respect to the homogeneous fluid provided $\beta\rho$ is high enough, they are no match for any of the direct phases, and *a fortiori* for the cluster phase which has the lowest free energy of them all. This is due to the fact that, as observed in Section III, for soft-core systems the free energy is dominated by its excess contribution. The quantity $q\psi(\lambda)/2$ which gives the strength of that contribution has been plotted as a function of λ in panel (a) of Fig. 8. For the lamellar phase, $\psi(\lambda)$ coincides with $\varphi(\pi - \lambda)$ because of the aforementioned invariance. However, for clusters and cylinders, the factor $[\lambda^d/(\alpha - \lambda^d)]^2$ strongly depresses $\psi(\lambda)$ with respect to $\varphi(\lambda)$, to the point that $q\psi(\lambda)$ lies always well below the corresponding quantity of the lamellae despite the lower q of the latter. The difference is even larger when $\psi(\lambda)$ is pitted against $\varphi(\lambda)$ for the same kind of aggregates, either clusters or cylinders, as shown by the comparison between Fig. 8 and Fig. 1 (please note that in Fig. 1 the factor q is not included, and that the difference is further amplified by including

it). Hence, for soft-core potentials inverted phases represent a poor strategy to minimize the free energy.

The reason why this is not always the case with hard-core potentials is due, once more, to the fact that in these systems it is imperative to counteract the growth of $\bar{\rho}$. According to Eq. (49), with inverted phases this can be achieved by decreasing λ as ρ increases. Hence, unlike what found for soft-core interactions, the size of the holes decreases on increasing ρ, so as to leave more room for particles. At this point, the relation $\alpha_{\mathrm{bcc}} \gg \alpha_{\mathrm{triang}} \gg \alpha_{\mathrm{1d}}$ comes into play: at given ρ, spherical holes allow one to obtain a similar value of $\bar{\rho}$ by a value of λ *substantially higher* than that necessary for cylindrical holes, which in turn allow for a substantially higher λ compared to lamellae. Since $\psi(\lambda)$ is an increasing function of λ, this gain in λ counterbalances the decrease in $q\psi(\lambda)$ at fixed λ as the dimension d of the holes is increased, and may tip the competition so as to favor the phase with larger d. This is shown more clearly in panel (b) of Fig. 8, where $q\psi(\lambda)/2$ has been plotted as a function of λ^d/α, so that for a certain ρ a given value of the abscissa corresponds to the same $\bar{\rho}$. When compared at the same $\bar{\rho}$, inverted cylinders become more favorable than lamellae as ρ is increased, and inverted spheres eventually become more favorable than inverted cylinders, as shown in the inset. At the transition to the inverted phase of higher dimensionality, λ and hence the hole size γ increases considerably [19].

Figure 6 reports the free energies per particle of the inverted cylinder and inverted spherical phases at $T^* = 0.022$ together with those of the direct phases, and shows the expected sequence spheres/cylinders/lamellae/inverted cylinders/inverted spheres on increasing ρ. One also notes that the free energies of the inverted phases are generally closer to each other, than either of them is to that of the lamellar phase.

VI. LIMITS OF THE THEORY

Besides the mean-field form (1) of the Helmholtz free energy upon which the whole theory rests, the other approximations introduced here are the assumption (4) that $\rho(\mathbf{r})$ can be represented by a sum of characteristic functions, and the truncation of the sum over neighbor shells of the reciprocal lattice in Eq. (25) at nearest neighbors. As for the latter approximation, its rationale is that in Eq. (25) the monotonically decreasing function $\varphi(\nu_i\lambda)$ acts as a form factor which depresses the contributions of the outer shells. If $\widetilde{w}(k)$ decays

rapidly enough and λ is relatively large, the decrease of $\varphi(\nu_i\lambda)$ from one shell to the next can be substantial enough to justify dropping all the shells from the second neighbor on. Therefore, for a given system the accuracy of the one-shell approximation depends in general on the behavior of λ as a function of the thermodynamic state.

As shown in Section III, for soft-core potentials λ is a decreasing function of $\beta\rho$. Indeed, for $\beta\rho \to \infty$ one has $\lambda \to 0$. In this limit, $\varphi(\nu_i\lambda) \to 1$ irrespective of ν_i, and in Eq. (25) the energetic contribution at $k \neq 0$ reduces to $\beta\rho S/2$, where S is the lattice sum

$$S = \sum_{\mathbf{k}\neq 0} \widetilde{w}(\mathbf{k}) = \sum_{i=1}^{\infty} n_i \widetilde{w}(\nu_i\kappa). \tag{55}$$

Hence, at large ρ or low T, the contribution of the outer cells is not screened by φ, and will in general be non negligible, depending on how quickly $\widetilde{w}(k)$ goes to zero for large k. Accordingly, the most stable phase may differ from the bcc predicted by the one-shell approximation. This situation is discussed in detail in Ref. [2], specifically with regard to the competition between the bcc and fcc phases, corresponding respectively to the fcc and bcc reciprocal lattices. Compared to the fcc, the bcc has a lower number of nearest neighbors, but its first- and second-neighbor shells are closer. Which of the two lattices probes more efficiently the region of the minimum of $\widetilde{w}(k)$ depends on the interaction. For the generalized exponential model of order four (GEM-4) considered in Ref. [2] such that $w(r) = \exp[-(r/\sigma)^4]$, the bcc reciprocal lattice does give a lower S, so that the fcc phase prevails at large $\beta\rho$. As observed in Ref. [2], for a different form of $w(r)$ one might find that the bcc phase is preempted by the fcc in the whole inhomogeneous region.

By the same token, in principle suitably chosen interactions might even stabilize bars or lamellae over cluster phases. This, however, is not the case for the GEM-4 potential, as can be concluded by calculating S and minimizing it with respect to κ for the bcc, triangular, and one-dimensional reciprocal lattices. In the inset to Fig. 3, the results for $\beta\rho S/2$ are compared with the one-shell approximation of Eqs. (31), (32) at large values of $\beta\rho$, where it reduces to Eq. (34). Clearly, the effect of including the outer shells of the reciprocal lattice is rather small, and does not change the balance between cluster, tubular, and lamellar phases with respect to what predicted by the one-shell approximation, notwithstanding the change in the lattice of the cluster phase. This situation is to be expected whenever the neighborhood of the minimum of $\widetilde{w}(k)$ accounts for the largest contribution to Eq. (55), even though such a contribution may result from two or even more reciprocal lattice shells. In this

respect, the larger coordination numbers attainable by three-dimensional lattices remains an advantage over lattices of lower dimensionality. In order to stabilize tubular or, *a fortiori*, lamellar phases, one could engineer the interaction so that $\widetilde{w}(k)$ would have narrow negative peaks at the reciprocal lattice vectors of the phase of lower dimensionality. This, however, looks like a rather *ad hoc* procedure.

Turning to hard-core potentials, we may point out as a preliminary observation that the mechanism behind the clusters/bars/lamellae sequence described in Section IV cannot be invoked to promote a transition from the bcc phase to more tightly packed cluster crystals. Let us consider for instance the fcc: for this lattice, the coefficient α which relates ρ with $\bar{\rho}$ according to Eq. (21) is given by

$$\alpha_{\mathrm{fcc}} = \frac{9\sqrt{3}\pi^2}{2} \simeq 76.9\,. \tag{56}$$

The comparison with Eq. (22) shows that $\alpha_{\mathrm{fcc}} < \alpha_{\mathrm{bcc}}$. However, the two values are similar, the relative difference amounting to less than 10%. This is to be contrasted with the decrease of α by a factor ~ 6 when going from the bcc to the triangular bar phase, and ~ 4.5 from the bar phase to the one-dimensional lamellar phase. Hence, the decrease in λ entailed by a transition from the bcc to the fcc phase is rather insubstantial, and does not compensate the decrease in the coordination number q of the reciprocal lattice. According to the one-shell approximation, the bcc phase would be always favored over the fcc.

As for soft-core potentials, the competition between the bcc phase and other three-dimensional cluster crystals is instead due to the contributions to Eq. (25) beyond nearest neighbors. According to the discussion of Sections IV and V, for hard-core potentials the dependence of λ on the thermodynamic state is not expressed any more by the sole quantity $\beta\rho$. At constant ρ, λ is an increasing function of T as in the soft-core case. We then expect that for each phase the effect of the outer shells of the reciprocal lattice will become more relevant on decreasing T.

This is qualitatively confirmed by the phase diagram of the SALR potential obtained by numerical minimization of functional (1) in Ref. [19], which we have reproduced in Fig. 9. In that study, we considered a hard-core two-Yukawa fluid (HCTYF) such that

$$w(r) = \frac{\sigma}{r}\left[-\epsilon e^{-z_1(r/\sigma-1)} + A e^{-z_2(r/\sigma-1)}\right] \tag{57}$$

with $z_1 = 1$, $z_2 = 0.5$, and $A/\epsilon = 7/19$. Please note that in Ref. [19] the reduced temperature

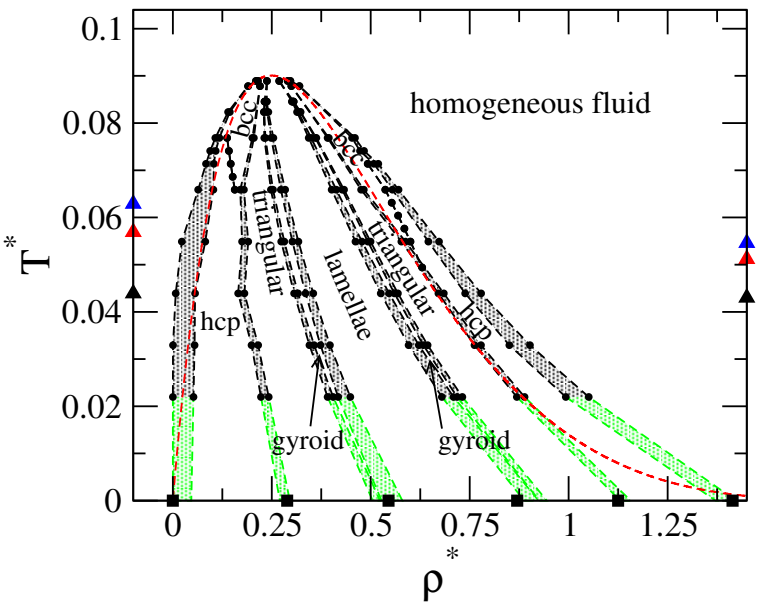

FIG. 9. Phase diagram of the HCTYF with $w(r)$ given by Eq. (57) and interaction parameters specified in the text in the temperature-density plane. The filled black circles represent the phase boundaries obtained in Ref. [19] by numerical minimization of functional (1). The black dashed lines are a guide for the eye. The grey shaded regions are coexistence domains. The green dashed lines and shaded regions denote the extrapolation of the phase diagram to $T = 0$, see Section VII. The filled squares refer to the transition densities at $T = 0$ given by Eqs. (69), (70) and (83)–(86). The red dashed line is the λ-line. The triangles along the left and right temperature axes display the threshold reduced temperatures $T^*_{\rm max}$ for the cluster, bar, and lamellar phases predicted by Eq. (45) (left), and estimated from Fig. 2 of Ref. [16] (right) for a SALR square-well plus ramp interaction. In both cases, black triangles refer to clusters, red triangles to bars, and blue triangles to lamellae.

was defined as $T^* \equiv k_{\rm B}T/\epsilon$, whereas here it has been rescaled according to Eq. (38) with w_0 given by $w_0 = 9.108\,\epsilon\sigma^3$.

Aside of the gyroid phase which we shall not be concerned with here, the phase diagram shows the expected sequence cluster/bars/lamellae/inverted bars/inverted clusters. However, instead of a single cluster (or inverted cluster) phase, we find both a bcc and a hcp phase. The hcp phase has nearly the same free energy as the fcc, and for the purpose of the present discussion the two lattices can be considered equivalent, even though the two-point basis of the hcp makes it more cumbersome to deal with. For the hcp, Eq. (11) is replaced

by

$$\frac{\beta F}{N} = f_{\rm ref}(\bar{\rho}) + \frac{\beta\rho}{2}\sum_{\mathbf{k}}\frac{1}{2}[1+\cos(\mathbf{k}\cdot\mathbf{r}_0)]\widetilde{w}(k)\varphi(\gamma k)\,, \tag{58}$$

where $\mathbf{k}$ runs over the sites of a hexagonal lattice with nearest-neighbor distance κ, and $\mathbf{r}_0$ is the vector of coordinates

$$\mathbf{r}_0 \equiv \left(\frac{\sqrt{6}\pi}{4\kappa}, \frac{\sqrt{2}\pi}{4\kappa}, \frac{\pi}{\kappa}\right)\,. \tag{59}$$

While for the fcc phase the (bcc) reciprocal lattice shells which contribute most to the free energy correspond to the first and second neighbors, for the hcp the contribution of the nearest-neighbor shell vanishes because of the phase factor in Eq. (58), and the most important contributions come from the second, third, and fourth-neighbor shells. Irrespective of these details, what we would like to point out here is that the more tightly packed lattice, be it fcc or hcp, prevails at low temperature, whereas at high temperature the bcc predicted by the one-shell approximation wins, in agreement with the expectation based on the behavior of λ.

The effect of the thermodynamic state on the accuracy of the one-shell approximation is represented more quantitatively in Fig. 10. The Figure reproduces panel (a) of Figs. 11, 12, and 13 of Ref. [19], and displays the wave vector $k_{\rm M}$ of the main Bragg peak of the cluster, bar, lamellar, inverted bar, and inverted cluster phases of the SALR HCTYF obtained by the numerical minimization of functional (1). In each panel, $k_{\rm M}$ has been plotted as a function of ρ along an isotherm, corresponding to $T^* = 0.077$, $T^* = 0.044$, and $T^* = 0.022$ for panels (a), (b), and (c) respectively, and compared to the wave vector k_0 of the minimum of $\widetilde{w}(k)$. As shown in Fig. 9, the cluster phase is bcc at $T^* = 0.077$, and hcp at $T^* = 0.044$ and $T^* = 0.022$. For the bar, lamellar, and cluster bcc phases $k_{\rm M}$ is equal to the wave vector κ of the nearest-neighbor shell of the reciprocal lattice. For the hcp phase, $k_{\rm M}$ is located at the third neighbor shell of the reciprocal lattice, and is almost identical to the κ of the fcc phase.

At $T^* = 0.077$, $k_{\rm M}$ is nearly density-independent and undistinguishable from k_0, in agreement with the prediction of the one-shell approximation, see Section II. As the temperature is lowered, the contributions to the free energy from reciprocal lattice vectors beyond nearest neighbors become more important, and the difference between $k_{\rm M}$ and k_0, albeit still remaining relatively small in absolute terms, nevertheless increases appreciably, with the cluster phases showing the largest deviations.

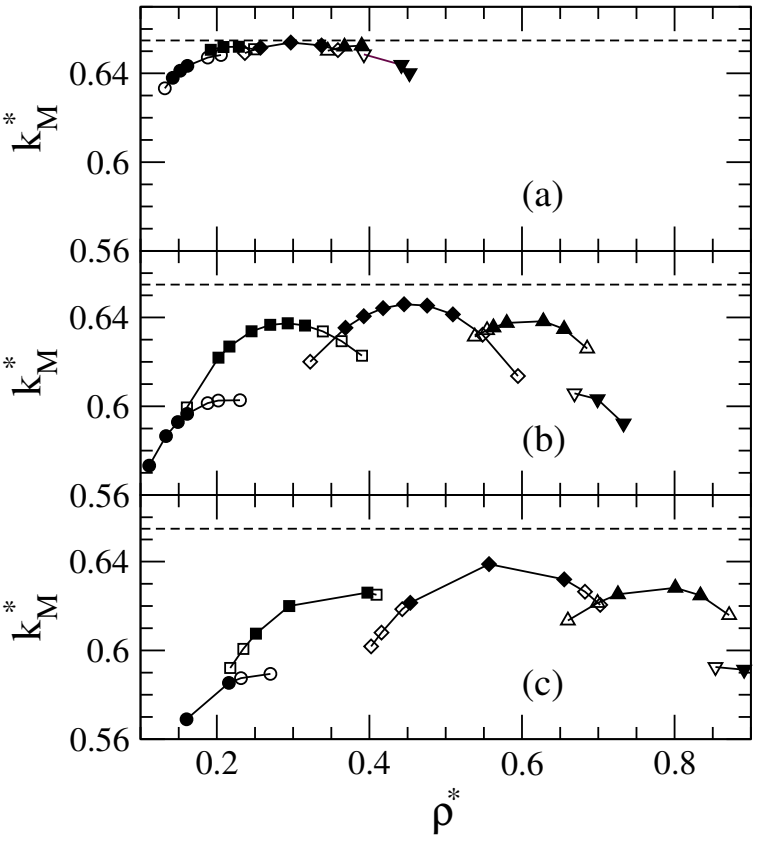

FIG. 10. Reduced wave vector $k_{\rm M}^*$ of the main Bragg peak of $\rho(\mathbf{r})$ as a function of reduced density obtained by the numerical minimization of functional (1) for the HCTYF of Eq. (57) with parameters specified in the text. Circles: spheres. Squares: cylinders. Diamonds: lamellae. Triangles up: inverted cylinders. Triangles down: inverted spheres. Filled symbols denote stable phases, whereas empty symbols denote phases that are either metastable or at coexistence. Lines are a guide for the eye. Panels (a), (b), and (c) refer to reduced temperatures $T^* = 0.077$, $T^* = 0.044$, and $T^* = 0.022$ respectively. The spherical cluster phase is bcc in panel (a) and hcp in panels (b) and (c). The dashed horizontal line represents the wave vector of the minimum of the Fourier transform of the tail potential $\widetilde{w}(k)$.

In Ref. [2], Likos *et al.* have suggested to quantify the relative weight of the second neighbor shell with respect to the first by the ratio Δ of the absolute values of the first two terms in the summation of Eq. (25), namely

$$\Delta = \frac{n_2|\widetilde{w}(\nu_2\kappa)|\varphi(\nu_2\lambda)}{q|\widetilde{w}(\kappa)|\varphi(\lambda)} \,. \tag{60}$$

We have evaluated Δ at $T^* = 0.022$ by feeding into Eq. (60) the values of κ and λ obtained

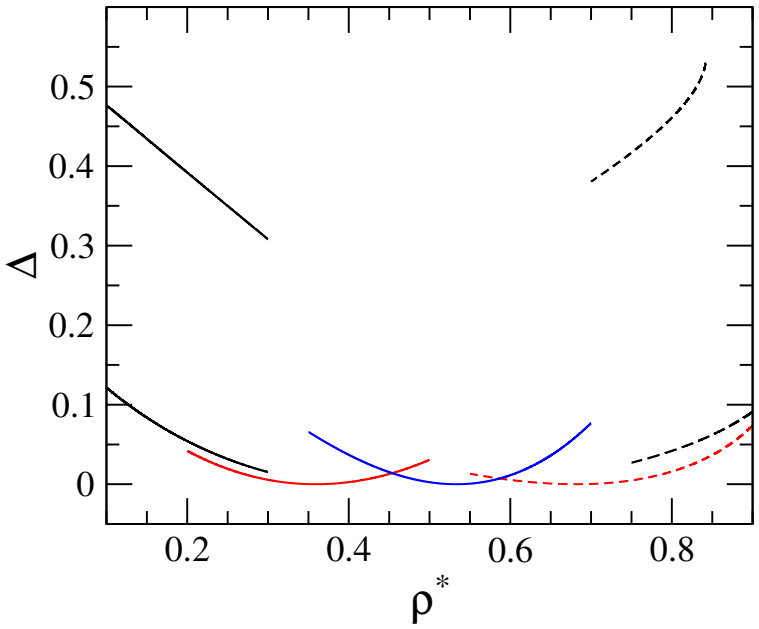

FIG. 11. Dimensionless ratio Δ defined in Eq. (60) as a function of reduced density at $T^* = 0.022$ for the HCTYF with parameters specified in the text. Solid black lines: spheres. Solid red line: cylinders. Solid blue line: lamellae. Dashed red line: inverted cylinders. Dashed black lines: inverted spheres. For spherical phases, the lower line refers to the bcc phase, and the upper line to the fcc phase.

from the one-shell approximation used throughout this study, so that the resulting quantity gives an indication of the consistency of the approximation. In Fig. 11, Δ for clusters, bars, lamellae, inverted bars, and inverted clusters is plotted as a function of ρ in intervals roughly corresponding to those of panel (c) of Fig. 10. For clusters, the curves corresponding to both bcc and fcc phases have been displayed. The latter has been chosen instead of the hcp so as to avoid the additional complication entailed by the phase factor in Eq. (58). The Figure shows that, on the one hand, the fcc phase has by far the largest Δ, in qualitative agreement with the behavior shown in Fig. 10: in order to explain the stability of the fcc (or hcp) phase, reciprocal lattice shells beyond the first must be considered. On the other hand, even at this relatively low temperature, the first shell accounts for most of the excess free energy of both the triangular bar and the lamellar phases, at least in the region where either phase is stable, and same applies to the metastable bcc phase.

The dependence of Δ on ρ is due to λ. We recall that at constant T, λ is an increasing function of ρ for direct phases, and a decreasing function of ρ for inverted phases. As the

density moves from the outer to the inner region of the phase diagram, $\nu_2\lambda$ increases and, since obviously $\nu_2 > 1$, it may exceed the upper bound for λ set by Eq. (20), and probe the domain where φ is non-monotonic. This is indeed the case for bars and lamellae, for which Δ reaches a vanishing minimum at densities such that $\varphi(\nu_2\lambda)$ vanishes. We observe that the minima of Δ do correspond to the rounded maxima of k_{M} exhibited by bars and lamellae in Fig. 10, for which k_{M} is closest to the value k_0 predicted by the one-shell approximation. For cluster phases, instead, $\varphi(\nu_2\lambda)$ does not vanish in the region where the phase is stable, and Δ is a monotonically decreasing or increasing function of ρ for the direct and inverted phase respectively. This behavior is consistent with the effect of ρ on the bcc-hcp transition at temperatures (higher than that of Fig. 11) at which both phases are present, see Fig. 9: for direct cluster phases, as ρ increases the contribution of the outer shells becomes smaller, and the bcc phase prevails. This should be contrasted with the situation found in soft-core potentials [2], where, more intuitively, on increasing ρ one goes from the more loosely to the more tightly packed lattice. For inverted clusters, Δ decreases on decreasing ρ, so that the bcc wins at lower ρ.

We may then say that, even though the one-shell approximation adopted here erroneously predicts that the bcc is always the most stable cluster phase, the dependence of λ on the thermodynamic state accounts qualitatively for the possibility that other, more tightly packed lattices can be favored. Nevertheless, this should not prevent us from pointing out the limits of this approach. Let us go back, in particular, to Eq. (45): according to it, the bcc cluster phase should appear for $T^* < 0.0439$. However, the phase diagram obtained by the numerical DFT minimization of the SALR HCTYF displayed in Fig. 9 shows that, in fact, for those values of T^*, the hcp phase already prevails in the whole cluster region. This state of affairs points at an inconsistency intrinsic to the present treatment: at temperatures low enough that the representation of $\rho(\mathbf{r})$ by characteristic functions makes sense, the contributions to the free energy due to the outer shells of the reciprocal lattice may well become substantial enough, that the bcc is no longer the preferred cluster phase. In this situation, a truncation of the excess free energy to nearest neighbors in *direct* space would probably be more accurate.

For the purpose of this study, such a deficiency is less serious than it sounds. Here we are not so much interested in the identification of the most stable lattice of cluster phases (or bar phases for that matter), as in elucidating the reason why the periodicity of these

phases changes from triple to double to simple and vice versa on increasing ρ, and why this pattern is common to many interactions which, when compared in real space, appear to be quite different. We believe that the mechanism described in Sections IV and V captures the essential ingredients behind such a pattern, irrespective of whether a specific cluster arrangement is stabilized by a single reciprocal lattice shell at k_0 as the bcc phase, or by two (or even more) shells in the neighborhood of k_0 as the fcc or hcp phases. Clearly, within the present approximation we *must* stick to the bcc lattice for $d = 3$ and to the triangular lattice for $d = 2$, because they are the most stable three- and two-dimensional lattices when only the first neighbor shell of the reciprocal lattice is taken into account, and for them the contributions of the other shells is indeed small, as shown in Fig. 11.

A conceptually more important issue is that, although this approach is clearly mean-field in nature, the assumption of a sharp interface for $\rho(\mathbf{r})$ is not consistent with the topology of the mean-field phase diagram at high temperature, according to which the coexistence domains should coalesce at the top of the λ-line, see Fig. 9. As discussed in Sec. IV, here instead we find that, on increasing the temperature, the cluster phase will be the first to disappear, to be followed by the bars, and finally by the lamellae.

Actually, the outcome of both numerical simulations [16] and theoretical methods in which fluctuations are taken into account [20] shows that the latter picture is the correct one, so that this might be considered as an asset rather than a liability. In this respect, it is interesting to compare the reduced temperatures $T^*_{\rm max}$ of Eq. (45) with the simulation results of Ref. [16], where a SALR fluid consisting of a square well and a repulsive ramp such that $w_0 = 9.586\,\epsilon\sigma^3$ was considered. The temperatures above which the lamellar, bar, and cluster phases disappear can be estimated from Fig. 2 of that study (please note that there the cluster phase is fcc rather than bcc), and converted into the reduced units adopted here via Eq. (38). This gives $T^*_{\rm max,\,fcc} = 0.043$, $T^*_{\rm max,\,triang} = 0.051$, and $T^*_{\rm max,\,1d} = 0.055$, in fair to good agreement with of Eq. (45). The two sets of values have also been displayed in Fig. 9.

However, here such a result is obtained, so to speak, as a compensation of two errors: on the one hand, fluctuations are disregarded by adopting a mean-field free energy functional. On the other hand, one enforces first-order phase transitions by imposing a step-like density profile quite different from that which the functional would spontaneouly choose at high temperature, if it were granted the freedom to do so. Clearly, a satisfactory description of mesophase formation should tackle both problems.

As a side remark, one cannot but notice that, as also observed in Ref. [20], in these systems fluctuations appear to play a much more important role, than they do in the liquid-vapor transition. In a Lennard-Jones like fluid, fluctuations depress the critical temperature by less than 10% with respect to the mean-field prediction [28]. In the present case, by contrast, the difference between the temperature T^*_λ below which mesophases should appear according to mean-field theory and the simulation result for $T^*_{\max,\,1\mathrm{d}}$ amounts to more than 60% of the latter.

In the next two Sections we shall use the approach discussed so far in a more quantitative way to obtain some predictions concerning the transitions between clusters and bars and bars and lamellae in the low-temperature regime, which is the best suited [26] to the representation of $\rho(\mathbf{r})$ by Eqs.(5)–(7). We are aware that, for each phase, the actual lattice may differ from that predicted here, but we expect that a more refined treatment, while leading to the correct identification of each lattice, would not alter significantly the balance between phases of different dimensionality.

VII. BEHAVIOR FOR $T \to 0$

Sections IV and V have highlighted the fundamental role of the hard-sphere free energy in generating the sequence of phases commonly observed in hard-core $Q^{\pm}$ potentials, as opposed to the situation in which particles are mutually penetrable. Let us now consider what this implies in the limit $T \to 0$.

If $Z_{\mathrm{ref}}(\bar\rho)/\bar\rho$ remains finite in this limit, then the r.h.s. of Eq. (43) vanishes, which implies either $\lambda = 0$ or $d = 1$, $\lambda = \pi$, see panel (a) of Fig. 4. The former solution is unphysical, since it gives a diverging density $\bar\rho$ inside the aggregates, while the latter corresponds to the homogeneous phase such that $\Delta F = 0$. Hence, in order to obtain a physical inhomogeneous phase with a negative ΔF, $Z_{\mathrm{ref}}(\bar\rho)/\bar\rho$ must diverge so as to compensate for the divergence of β. The divergence issuing from $\bar\rho = 0$ is to be discarded, since it implies $\rho = 0$. This leaves as the only possibility the divergence of $Z_{\mathrm{ref}}(\bar\rho)$, which occurs at the close-packing density $\rho^*_{\mathrm{cp}} = \sqrt{2}$. Therefore, as $T \to 0$, $\bar\rho$ must approach ρ_{cp}. As observed at the beginning of Section IV, Eq. (36) for $Z_{\mathrm{ref}}(\bar\rho)$ is actually unaware of close packing and, although it does diverge at high density, it places the divergence at the unphysically high value $\eta = 1$. If we assume that the functional form of $Z_{\mathrm{ref}}(\bar\rho)$ in the neighborhood of close packing is

still described by Eq. (36) provided its pole is moved at the physical close packing, the requirement that the r.h.s. of Eq. (43) be of order 1 as $T \to 0$ leads to

$$\beta \sim \frac{1}{(\rho_{\rm cp} - \bar{\rho})^3}\,, \tag{61}$$

while Eq. (35) for $f_{\rm ref}(\bar{\rho})$ gives

$$f_{\rm ref}(\bar{\rho}) \sim \frac{1}{(\rho_{\rm cp} - \bar{\rho})^2}\,. \tag{62}$$

It may be argued that such an assumption is unjustified. In fact, more accurate calculations of the equation of state [29] predict a simple pole for $Z_{\rm ref}(\bar{\rho})$ at close packing. Equations. (61), (62) should then be replaced by

$$\beta \sim \frac{1}{\rho_{\rm cp} - \bar{\rho}}\,, \tag{63}$$

$$f_{\rm ref}(\bar{\rho}) \sim -\ln(\rho_{\rm cp} - \bar{\rho})\,. \tag{64}$$

However, the precise form of the divergence is not important here as long as $Z_{\rm ref}(\bar{\rho})$ has some kind of power-law divergence for $\bar{\rho} \to \rho_{\rm cp}$, such that the divergence of $f_{\rm ref}(\bar{\rho})$ in the same limit is weaker. As a consequence, as shown by both Eqs. (61), (62) and (63), (64), the divergence of β as a function of $\bar{\rho}$ is stronger than that of $f_{\rm ref}(\bar{\rho})$. If Eq. (28) for ΔF is divided by β, then both $f_{\rm ref}(\bar{\rho})$ and, *a fortiori*, $f_{\rm ref}(\rho)$ disappear in the limit $T \to 0$, and we obtain

$$\frac{\Delta F_{T=0}}{N} = -\frac{q w_0}{2} \rho\, \varphi(\lambda)\,, \tag{65}$$

where the value of λ is determined by setting $\bar{\rho} = \rho_{\rm cp} = \sqrt{2}/\sigma^3$ in Eq. (21) so that

$$\lambda = \left(\frac{\alpha \rho^*}{\sqrt{2}}\right)^{1/d}\,. \tag{66}$$

If we turn to the inverted phases and divide Eq. (50) by β, we find

$$\frac{\Delta F_{T=0}}{N} = -\frac{q w_0}{2} \rho\, \psi(\lambda)\,, \tag{67}$$

where λ is given by Eq. (49) with $\bar{\rho} = \rho_{\rm cp}$:

$$\lambda = \left[\alpha\left(1 - \frac{\rho^*}{\sqrt{2}}\right)\right]^{1/d}\,. \tag{68}$$

Hence, at $T = 0$ the Helmholtz free energy reduces to its purely energetic part, as one would expect. However, the legacy of the hard-core entropic part is still contained in the condition $\bar{\rho} = \rho_{\rm cp}$ that determines λ.

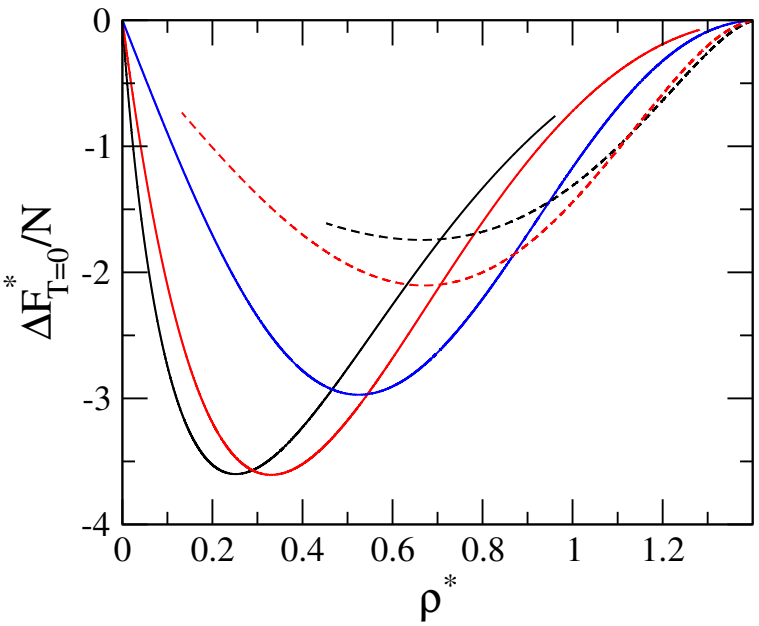

FIG. 12. Difference $\Delta F^*_{T=0}$ between the reduced Helmholtz free energy $F^* \equiv F\sigma^3/w_0$ of the inhomogeneous phase and that of the homogeneous fluid for hard-core $Q^{\pm}$ fluids at $T = 0$. Lines as in Fig. 6.

Clearly, according to Eqs. (66), (68) the size of the aggregates of the direct phases increases with ρ, while the size of the holes of the inverted phases decreases with ρ, as for $T \neq 0$. The sequence of phases is then determined by the same mechanism discussed in Sections IV, V, and remains unaltered. This is shown in Fig. 12, where the quantity $\Delta F_{T=0}/N$ given by Eqs. (65), (67) has been plotted as a function of density for all the phases considered in this study. We recall that for direct phases, the upper limit on λ set by Eq. (20) together with Eq. (66) determine an upper limit $\rho^{\rm B}$ on ρ^* given by Eqs. (40)–(42). Similarly, for inverted phases Eqs. (20) and (68) determine a lower limit on ρ^* given by $\sqrt{2} - \rho^{\rm B}$, with $\rho^{\rm B}$ expressed again by Eqs. (40)–(42). The Figure also shows that at $T = 0$ the inhomogeneous region spans the whole density axis from zero to close packing, as obtained straightforwardly by setting $\Delta F_{T=0} = 0$ in Eqs. (65), (67). For Eq. (65), this condition is met by

$$\rho^*_{\rm fluid-bcc} = 0\,, \tag{69}$$

which because of Eq. (66) implies $\lambda = 0$. For Eq. (67), the same condition is satisfied by having $\psi(\lambda)$ vanish, which again gives $\lambda = 0$ and hence by virtue of Eq. (68)

$$\rho^*_{\rm bcc'-fluid} = \sqrt{2}\,. \tag{70}$$

We remark that this does not imply that at $T = 0$ mesophases will still exist down to $\rho = 0$ or up to $\rho = \rho_{\rm cp}$. Indeed, at such densities their free energy might not even be convex, and one expects coexistence between phases with different ρ. What Eqs. (69), (70) indicate is that on the low- and high-density side of the phase diagram, the mesophases coexist respectively with a gas of vanishing ρ and with an atomic crystal [17].

Interestingly, at $T = 0$ we can obtain simple expressions for the size of clusters, bars, lamellae and the corresponding inverted domains at the phase boundary. As just stated, such a boundary is actually a coexistence region with a non vanishing amplitude in density, but in the following we shall disregard this, and assume that at the transition between two phases A and B we may estimate the coexistence density by setting $\rho_A = \rho_B = \rho_\times$, where $\rho_\times$ is the density at which the Helmholtz free energies of those phases coincide. Equation (66) then implies

$$\lambda_B = \left(\frac{\alpha_B}{\alpha_A} \lambda_A^{d_A} \right)^{1/d_B} . \tag{71}$$

If we impose the equality of the free energies of the two phases, Eq. (65) gives

$$q_A \varphi_A(\lambda_A) = q_B \varphi_B \left[\left(\frac{\alpha_B}{\alpha_A} \lambda_A^{d_A} \right)^{1/d_B} \right] , \tag{72}$$

where we have used Eq. (71) to express λ_B in terms of λ_A. By using Eqs. (12)–(14) for $\varphi(\lambda)$ and Eqs. (22)–(24) for α, we find

$$\lambda_{\rm bcc}^{\rm bcc-triang} = 2.577 \quad \lambda_{\rm triang}^{\rm bcc-triang} = 1.722 \,, \tag{73}$$

$$\lambda_{\rm triang}^{\rm triang-1d} = 2.364 \quad \lambda_{\rm 1d}^{\rm triang-1d} = 1.210 \,, \tag{74}$$

where Eq. (73) refers to the transition between the bcc cluster and the triangular bar phases, and Eq. (74) to that between the triangular bar and lamellar phases.

The above results are straightforwardly extended to the inverted phases. Because of Eq. (68), setting $\rho_{\rm A} = \rho_{\rm B}$ implies that the sizes of the holes $\lambda_{\rm A}$, $\lambda_{\rm B}$ are related by Eq. (71), just as the sizes of the aggregates of the "direct" phases. Moreover, the factor $\lambda^d/(\alpha - \lambda^d)$ in the r.h.s. of Eq. (51) is, once more, the same for the two phases. As a consequence, by equating the free energies given by Eq. (67), one finds again Eq. (72). If we denote by a prime the inverted phases at the transition, we have then

$$\lambda_{\rm triang'}^{\rm triang'-bcc'} = \lambda_{\rm triang}^{\rm bcc-triang} \quad \lambda_{\rm bcc'}^{\rm triang'-bcc'} = \lambda_{\rm bcc}^{\rm bcc-triang} \,, \tag{75}$$

$$\lambda_{\rm 1d'}^{\rm 1d'-triang'} = \lambda_{\rm 1d}^{\rm triang-1d} \quad \lambda_{\rm triang'}^{\rm 1d'-triang'} = \lambda_{\rm triang}^{\rm triang-1d} \,, \tag{76}$$

so that at the phase boundaries the size of the filled domains of the "direct" phases, be they clusters, bars, or lamellae, is predicted to be the same as that of the holes of the corresponding inverted phases. For the lamellae, it is perhaps more natural to consider the size of the filled domains instead of that of the holes also for the inverted phase. As observed in Section V, the two are related by $\lambda = \pi - \lambda'$. Therefore, we find

$$\lambda_{\rm 1d}^{\rm 1d-triang'} = \pi - \lambda_{\rm 1d'}^{\rm 1d'-triang'} = 1.932\,. \tag{77}$$

We recall that the half-width γ of the aggregates is related to λ by $\gamma = \lambda/\kappa$ and that in the present approximation we have $\kappa = k_0$, where k_0 is the wave vector of the minimum of $\widetilde{w}(k)$. The dependence of the values of γ at the transition on the specific form of the interaction then enters *only* via k_0.

A set of interaction-independent values can be obtained by considering the ratio between γ at the transition and the nearest-neighbor distance in real space a. Since $a = \theta/\kappa$ with θ given by Eqs. (17)–(19), we find $\gamma/a = \lambda/\theta$, which, like λ, depends only on the kind of equilibrium one is considering:

$$(\gamma/a)_{\rm bcc}^{\rm bcc-triang} = (\gamma/a)_{\rm bcc'}^{\rm triang'-bcc'} = 0.335 \tag{78}$$

$$(\gamma/a)_{\rm triang}^{\rm bcc-triang} = (\gamma/a)_{\rm triang'}^{\rm triang'-bcc'} = 0.237\,, \tag{79}$$

$$(\gamma/a)_{\rm triang}^{\rm triang-1d} = (\gamma/a)_{\rm triang'}^{\rm 1d-triang'} = 0.326\,, \tag{80}$$

$$(\gamma/a)_{\rm 1d}^{\rm triang-1d} = 0.193\,, \tag{81}$$

$$(\gamma/a)_{\rm 1d}^{\rm 1d-triang'} = 0.307\,, \tag{82}$$

where the last two values refer to the size of the lamellae for the equilibrium between bars and lamellae and between lamellae and inverted bars respectively. According to the above result, when a direct phase appears, the half-size γ of its aggregates is $\sim 1/5$ of the nearest-neighbors distance a, and as ρ is increased it grows to $\sim 1/3$ of this distance, at which point another phase takes over. Conversely, for inverted phases the half-size of the holes shrinks to $\sim a/3$ to $\sim a/5$ on increasing ρ. This implies that neither aggregates nor holes ever achieve the maximum packing $\gamma = a/2$.

Finally, if we substitute the above values of λ into Eqs. (66), (68) and solve with respect

to ρ^*, we obtain for the transtion densities at $T = 0$

$$\rho^*_{\mathrm{bcc-triang}} = 0.289\,, \tag{83}$$

$$\rho^*_{\mathrm{triang-1d}} = 0.545\,, \tag{84}$$

$$\rho^*_{\mathrm{1d-triang'}} = 0.870\,, \tag{85}$$

$$\rho^*_{\mathrm{triang'-bcc'}} = 1.125\,. \tag{86}$$

which are again independent of the interaction.

In order to assess the reliability of this prediction, we have turned to the phase diagram obtained by numerical minimization of functional (1) for the SALR HCTYF of Ref. [19], and extrapolated its phase boundaries to $T = 0$. Even though extrapolation is always questionable, we chose to do so instead of pushing the numerical minimization to extremely low temperatures. The reason for this is that the hard-sphere fluid in the reference term of functional (1) has been described by the Carnahan-Starling expressions (35), (36), and therefore is unable to handle properly the close packing of particles within the aggregates which, as highlighted throughout this Section, has to be taken into account as $T \to 0$. The unphysical behavior of the Carnahan-Starling equation of state at very low temperatures is apparent from the λ-line shown in Fig. 9, which extends well beyond the physical close packing. In this respect, extrapolating to $T = 0$ the numerical results obtained at temperatures such that Eqs. (35), (36) are still reliable looks like a safer procedure.

The comparison with the results thus obtained and those of Eqs. (83)–(86) is displayed again in Fig. 9. Aside of the extrapolation, there is some degree of uncertainty due to the fact that the width of the coexistence regions is non negligible, unlike what assumed in the present calculation. Moreover, the coexistence domain between lamellae and bars (or inverted bars) is actually split into a lamellae-gyroid and a gyroid-bar domain because of the gyroid phase, which has been disregarded here. Having said so, the agreement between the two sets of results is surprisingly good. We also note that extrapolation to $T = 0$ of the high-density phase boundary between inverted clusters and homogeneous fluid does correspond to the physical close packing, in agreement with Eq. (70). This is remarkable, given that no notion of it is contained in the free-energy functional. Nevertheless, we do not expect that the inverted cluster phase will actually persist at arbitrarily low temperatures, since according to Eq. (86), at $T = 0$ this phase should appear at densities higher than the freezing density of the hard-sphere fluid. Hence, below some temperature it will be most

likely preempted by freezing, and the atomic crystal will coexist with a mesophase of lower dimensionality.

VIII. AGGREGATE SIZE AT THE TRANSITIONS

It is tempting, albeit somewhat hazardous, to surmise that the relations obtained in Section VII for the size of coexisting aggregates at $T = 0$ may be applied also at $T \neq 0$. If we identify as before the densities at coexistence $\rho_\times$ between phases A and B at a given temperature with that at which the Helmholtz free energies of those phases coincide, $\rho_\times$ and the dimensionless sizes λ_A and λ_B of the phases at the transition are determined by equating the free energies of Eq. (28) for the two phases, and solving numerically this condition together with the two equations obtained by substituting into Eq. (30) $\rho_\times$, λ_A and $\rho_\times$, λ_B respectively. Instead of doing so, we shall *assume* that the densities $\bar{\rho}$ inside two aggregates at the transition are very similar, to the point that their differences can be neglected. As shown before, this assumption is actually correct in the limit of vanishing temperature, when $\bar{\rho}$ always goes to $\rho_{\rm cp}$. At low but non vanishing temperature, it is a further approximation on the top of those already introduced in the present treatment. Its rationale lies in the fact that, except at very low density, $\bar{\rho}$ is a rather slowly varying function of ρ, and as ρ is increased it reaches a plateau whose height depends weakly on the kind of aggregate. In fact, as observed above, at $T \neq 0$ it is the necessity to prevent $\bar{\rho}$ from growing too much that prompts the kind of phase behavior observed in $Q^{\pm}$ hard-core fluids. Two phases with very different values of $\bar{\rho}$ could hardly coexist with each other, since the phase at lower $\bar{\rho}$ would always have the lower free energy.

Under this assumption, at the transition we have then not only $\rho_A = \rho_B$, but also $\bar{\rho}_A = \bar{\rho}_B$. This leads again to Eq. (71). Moreover, when imposing the equality of the free energies, the reference terms in Eq. (28) can be dropped, since they are evaluated at the same densities for both phases, and one gets again Eq. (72). Therefore, we obtain once more Eqs. (73), (74) for the values of λ at the transition, irrespective of the values of $\rho_\times$. The latter cannot be obtained from Eqs. (71), (72) since they do not contain the density and, unlike in the $T = 0$ case, now $\bar{\rho}$ is not known *a priori*. If we turn to the inverted phases and assume again the same value of $\bar{\rho}$ for the density outside the empty domains of two phases at the transition, we can similarly drop the reference terms in Eq. (50), and by going through the same line

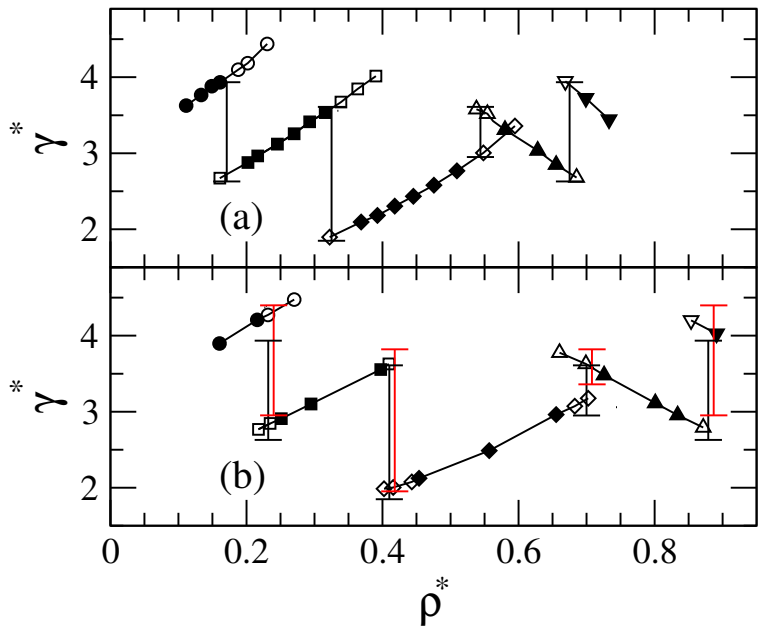

FIG. 13. Points: reduced half-width γ^* of the aggregates as a function of the reduced density ρ^* for the HCTYF of Eq. (57) with parameters specified in the text obtained by numerical DFT minimization at $T^* = 0.044$ (panel (a)) and $T^* = 0.022$ (panel (b)). Symbols as in Fig. 10. Vertical black bars: results for $\gamma^* = \lambda/\kappa^*$ at the transition according to Eqs. (73)–(77) with $\kappa^* = k_0^* = 0.655$. Red vertical bars in panel (b): results for γ^* obtained from Eqs. (87). Red bars have been given a small horizontal offset to make them more easily distinguishable.

of reasoning put forth in Section VII, we find once more Eqs. (75)–(77) relating the size of the holes to that of the aggregates of the direct phases.

We have tested Eqs. (73)–(77) by determining the half-width $\gamma = \lambda/k_0$ for the SALR HCTYF of Eq. (57), for which the wave vector k_0 of the minimum of $\widetilde{w}(k)$ is $k_0^* = 0.655$ in reduced units. If at all, the resulting values are expected to hold at low temperature since, as discussed in Section VI, the modelization of mesophases as compact objects is justified only in this regime. As one approaches the maximum temperature for mesophase formation, it even makes little sense to talk about the size of the aggregates, since $\rho(\mathbf{r})$ is more akin to a periodic modulation of a uniform background.

Figure 13 reproduces panel (c) of Figs. 12 and 13 of Ref. [19]. In panel (a) we have plotted γ as a function of density determined as the half width at half maximum of the density peaks obtained from the numerical minimization of functional (1) at $T^* = 0.044$, about half the value at the top of the coexistence region. At the densities at which phase coexistence occurs

according to the numerical calculation, we have also displayed the predictions for γ given by Eqs. (73)–(77). In the light of all the approximations involved, the agreement is remarkable, to the point that it raises a feeling of suspicion and calls for further checks. Accordingly, in panel (b) we have displayed a similar comparison for $T^* = 0.022$, which is the lowest temperature investigated numerically in Ref. [19]. We see that the agreement between the numerical result and the prediction of Eqs. (73)–(77) gets worse, especially for the cluster-bar and inverted cluster-inverted bar transitions. Since the modelization of the density profile as a sum of characteristic functions is expected to become more accurate as T gets smaller, this loss of accuracy could be traced back to some of the other approximations made, either the truncation of the excess free energy at the nearest-neighbor shell in reciprocal space, or the additional assumption $\bar{\rho}_A = \bar{\rho}_B$ for two phases A and B at the transition. As discussed in Section VI, the one-shell approximation is indeed expected to become less accurate at low T. In fact, at both temperatures considered in Fig. 13, the lattice of the cluster and inverted cluster phases is hcp, whereas Eq. (28) gives the bcc as the most stable lattice. This means that at these temperatures the contribution to the free energy given by shells beyond nearest neighbors in reciprocal space in non negligible.

The calculation can be straightforwardly generalized to include this contribution, provided the hypothesis $\bar{\rho}_A = \bar{\rho}_B$ for the phases at the transition is maintained. In this case, imposing the equality of the free energies gives

$$\sum_{i=1}^{\infty} n_i^A \widetilde{w}(\nu_i^A \kappa^A) \varphi_A(\nu_i^A \lambda) = \sum_{i=1}^{\infty} n_i^B \widetilde{w}(\nu_i^B \kappa^B) \varphi_B(\nu_i^B \lambda) \,. \tag{87}$$

We remark that now the nearest-neighbor distance in reciprocal space κ does not coincide any more with the wave vector k_0 of the minimum of $\widetilde{w}(k)$, and has to be determined by solving Eq. (26) for both phases. This can be done via Raphson-Newton iteration starting from an initial guess for κ, e.g. $\kappa_0 = k_0$. Strictly speaking, Eq. (87) holds for a simple Bravais lattice, whereas the hcp lattice formed by the cluster and inverted cluster phases has a two-point basis. In this case, Eq. (11) is replaced by Eq. (58), and Eq. (87) is modified accordingly. For the purpose of the present discussion, one might as well replace the hcp lattice with the fcc, and stick to Eq. (87), since the results for the two lattices are found to be undistinguishable for any practical matter.

The wave vectors κ^A, κ^B at the transition as well as the sizes of the coexisting aggregates are still predicted to be state-independent, just as in the simpler treatment based on Eq. (72).

However, the dimensionless size λ now depends on the specific form of the interaction. This is true *a fortiori* for γ, whose dependence on the interaction is not conveyed any more by the sole wave vector k_0. Moreover, the independence of κ^A, κ^B on the thermodynamic state granted by the assumption $\bar{\rho}_A = \bar{\rho}_B$ pertains only to the transition between two specified phases. As discussed in Section VI, when contributions beyond nearest neighbors are included in Eq. (26), κ will be in general state-dependent.

For the SALR HCTYF in hand, the values of γ thus obtained have been displayed in panel (b) of Fig. 13 together with those given by Eqs. (73)–(77). The comparison does not show a clear overall improvement, but rather that, while the values of Eqs. (73)–(77) underestimate the results of the numerical minimization, those obtained by solving Eq. (87) overestimate them. As T is lowered, there is a definite trend for γ to move towards the values predicted by Eq. (87) which, however, at $T^* = 0.022$ is still in progress. This indicates that, even at such a low temperature, the relation $\bar{\rho}_A = \bar{\rho}_B$ expected to hold at $T \to 0$ is only approximately satisfied, as can be checked directly on a plot of $\bar{\rho}$ vs. ρ. Hence, the remarkable performance of Eqs. (73)–(77) in panel (a) has to be considered an accident due to a compensation of errors. As T is lowered, an agreement of the kind displayed in panel (b) is more realistic.

Notwithstanding the above considerations, it is fair to point out that the discrepancy between the two sets of γ amounts to $\sim 10\%$. Since the actual γ are bracketed by these sets, such a difference, although far from being undetectable, is not very important for the purpose of getting a sensible estimate of the size of the aggregates. In this respect, the simpler treatment based on Eq. (72) leading to Eqs. (73)–(77) has the advantage of embodying the dependence on the interaction only via k_0.

IX. CONCLUSIONS

We have investigated the formation of periodic mesophases in fluids with hard-core plus tail interactions. This study does not aim at a detailed description of the phase diagram for a specific choice of the interaction such as that carried out in Ref. [19] for the hard-core two-Yukawa fluid (HCTYF) with competing short-range attractive and long-range repulsive (SALR) forces. Instead, its purpose is mostly qualitative, i.e., to explain why a common pattern for the phase diagram is found for interactions which are apparently quite different,

such as the aforementioned SALR potential [11, 13, 15, 16, 18] and potentials featuring purely repulsive shoulders [12, 26] with no competing attraction. In all of those cases, mesophases are found only below a certain temperature, and as the density is increased at constant temperature, they follow a common sequence ranging from clusters to bars, lamellae, inverted bars, and inverted clusters.

The method which we have adopted is similar to that developed in Ref. [2] for soft-core potentials, and is based on a simple free-energy functional, whereby the hard-core part of the interaction is treated in local-density approximation, while mean-field approximation is used for the off-core contribution. In order to keep the theory analytically tractable, the density profile $\rho(\mathbf{r})$ is described by a given functional form depending on two parameters, which determine the width and mutual distance of the density peaks, and the off-core part of the free energy is truncated at the nearest-neighbor shell of the reciprocal lattice. Following the strong-segregation limit expected to hold at low temperature, the peaks of $\rho(\mathbf{r})$ have been represented by characteristic functions in the shape of spherical clusters, cylindrical bars, or flat lamellae.

The resulting description is admittedly oversimplified, and misses a number of important points: for one thing, disregarding the contributions of the outer shells in the reciprocal space may not lead to the correct identification of the most stable lattice, since it necessarily privileges, for each dimensionality of the density modulations, the reciprocal lattice with the highest number of nearest neighbors. Moreover, it rules out the possibility of describing bicontinuous structures such as the gyroid phase, which is found in a narrow region between the lamellar and bar (or inverted bar) phases. As is well known [11, 13, 30], in order to recover this phase, the free energy must take into account at least the first two neighbor shells of the reciprocal lattice. Even more importantly, although the theory does reproduce the sequence of phases as observed in numerical simulations [16], the assumption that mesophases can be described by a density profile which is either constant or vanishing is bound to become unrealistic as the temperature is raised.

Nevertheless, in our opinion the theory achieves the task for which it has been introduced: first, it incorporates the information according to which the essential ingredient leading to mesophases is that the Fourier transform of the tail potential $\widetilde{w}(k)$ has its absolute minimum at a non vanishing wave vector k_0 so as to favor density modulations of period $\sim 2\pi/k_0$. Of course, this notion is far from being new, as it has long been acknowledged not only for

soft-core [1, 2], but for hard-core interactions as well. However, in the latter case it has been mostly implemented within Landau-Brazovskiĭ effective free-energy functionals [11, 13, 20] or lattice models [12], rather than within a microscopic theory such as that developed in Ref. [2] for soft-core potentials, of which the present treatment can be considered the counterpart for hard-core systems. There are certainly other ways to develop a theory of mesophase formation in these systems, most notably in the strong-segregation limit, by integrating *a la* Hamaker the microscopic interaction over the volume of the spheres, bars, and lamellae so as to obtain the effective potentials between the aggregates [26]. Notwithstanding the usefulness and accuracy of this method, we deemed it unsuited for our purpose of getting a general picture of the process, because the resulting expressions, even assuming that they can be handled analytically, are involved, highly dependent on the microscopic interaction, and do not bring forward the link between the shape of the interaction in Fourier space and the attitude to form mesophases.

Moreover, the present description does explain why the cluster/bar/lamellae sequence takes place, why inverted phases occur, and why neither of these features are found in purely soft-core systems. In both soft- and hard-core mesophase-forming fluids, the distance between neighboring aggregates is, to a large extent, determined by k_0, so that its dependence on the average density ρ is weak or altogether negligible [1, 2]. As a consequence, an increase in ρ is obtained not by creating more aggregates, but by increasing their population. Soft- and hard-core systems differ in the way by which they pursue this task, the key point being the behavior of the *local* density $\bar{\rho}$ inside the aggregates as the average density ρ increases.

For soft-core systems, the entropic contribution to the free energy per particle increases very slowly with $\bar{\rho}$, and there is no need to control its growth. As ρ increases, $\bar{\rho}$ increases unboundedly, the size of the aggregates γ becomes arbitrarily small, and the free energy is more and more dominated by the internal energy, which favors higher-dimensionality cluster phases because of the higher number of neighbors q of their reciprocal lattice.

This scenario does no longer take place in hard-core systems where, as ρ is increased, $\bar{\rho}$ must increase at a much lower rate or even remain nearly constant [19] in order to prevent the singular entropic term from increasing beyond control. Hence, γ must increase with ρ, and this determines the decrease of the form factor φ of the aggregates, which is a decreasing function of γ via its dimensionless argument $\lambda = \gamma k_0$. Such a situation prompts a competition in the internal energy per particle: on the one hand, periodic phases with lower

dimensionality, such as bars or lamellae, are disfavored by the lower coordination number q of their reciprocal lattice. On the other hand, they are favored by the slower decrease of their form factor. This is not due to the differences between the form factors themselves which are, in fact, quite similar to one another, but rather to the different values of their arguments. Specifically, phases with lower dimensionality pack more efficiently, so that for a certain value of ρ, a value of $\bar{\rho}$ similar, or even smaller than that required by aggregates of higher dimensionality is obtained by narrower aggregates with a smaller γ, a smaller λ, and hence a larger φ. For each phase, the (negative) internal energy per particle is initially dominated by ρ and decreases as ρ increases, but at large ρ the decrease of φ prevails, and the internal energy starts increasing, i.e., it becomes smaller in absolute value. Eventually, by moving to a phase of lower dimensionality the decrease in q is overcompensated by the larger φ, and the transition takes place. Conversely, for inverted phases the form factor is an *increasing* function of the size of the empty regions. As a consequence, at high density holes of higher dimensionality are favored, since they allow to obtain a given $\bar{\rho}$ by a *larger* γ.

Hence, even at risk of oversimplifying, we may say that the sequence of phase transitions commonly observed in mesophase-forming hard-core fluids is driven by the internal energy, but the behavior of the internal energy rests crucially on the dependence of the mesophase size γ on ρ, which is ultimately dictated by entropy. This is particularly evident in the limit $T \to 0$, in which the free energy reduces to its energetic part, but γ is determined by the requirement that $\bar{\rho}$ must coincide with the density at close packing.

In addition to the qualitative considerations above, we have determined the threshold temperatures for the formation of cluster, bar, and lamellar phases, and found that they compare rather favorably with those obtained in a recent simulation study of a square-well plus ramp SALR potential [16]. Moreover, we have employed the scheme presented here to obtain some quantitative results in the aforementioned limit $T \to 0$. One result concerns a rough estimate of the reduced densities at the transition between different mesophases, which are predicted to attain the same values for any hard-core system, irrespective of the form of the tail interaction which causes the formation of the mesophases. The other one concerns the sizes γ of the coexisting mesophases, which are predicted to depend on the interaction only via the wave vector k_0 of the minimum of $\widetilde{w}(k)$, so that universal quantities are again obtained by expressing them by in units of $1/k_0$ via the dimensionless quantity λ

or, equivalently, in units of the nearest-neighbor distance of the direct lattice. The latter result can be extended to $T \neq 0$ under the assumption that $\bar{\rho}$ is roughly the same at the transition between different phases.

Clearly, the "universality" of these predictions does not rest on any deep reason, but just on the approximation used to obtain them, whereby the interaction enters only via its minimum at k_0. Nevertheless, we felt that they deserved at least to be tested. To this end, we compared them to the results presented in Ref. [19] for the phase diagram of the SALR HCTYF obtained by numerical minimization of the free-energy functional. Extrapolation of the phase diagram of Ref. [19] to $T = 0$ shows a surprising agreement with the densities obtained here. At the same time, it also shows that these values are of little use at $T \neq 0$, since the phase boundaries deviate appreciably from them as the temperature is raised, especially at high density. As for the predictions on γ, they were compared directly with the results of the numerical minimization at low temperature and the deviations, although far from being unappreciable, were found to be at most of the order of $\sim 10\%$. Hence, they may be of some usefulness also at $T \neq 0$, provided T is still low enough that regarding the aggregates as objects with a given size makes sense. A feature of these predictions which we consider attractive is that they do not rely on the detailed shape of the interaction, and do not try to explain the equilibrium size of the aggregates in terms of the interplay between its components in real space. The latter may not be quite obvious, especially when it is unclear how those components should be identified, as in the case of purely repulsive interactions.

It could then be worthwhile to check if the above numerical values for the size of the coexisting phases remain predictive also for other systems besides the SALR HCTYF of Ref. [19] which was considered here for comparison, such as the SALR fluid simulated in Ref. [16]. Moreover, numerical values corresponding to those presented here can be straightforwardly obtained also for mesophase-forming hard-core two-dimensional systems, for which a number of results have been obtained both at vanishing [25] and non vanishing [6, 10] temperature.

CONFLICTS OF INTEREST

There are no conflicts to declare.

---

[1] B. M. Mladek, D. Gottwald, G. Kahl, M. Neumann, and C. N . Likos, Phys. Rev. Lett. **96**, 045701 (2006); *ibid.* **97**, 019901 (2006).

[2] C. N. Likos, B. M. Mladek, D. Gottwald, and G. Kahl, J. Chem. Phys. **126**, 224502 (2007).

[3] B. M. Mladek, G. Kahl, and C. N. Likos, Phys. Rev. Lett. **100**, 028301 (2008); D. A. Lenz, B .M. Mladek, C. N. Likos, G. Kahl, and R. Blaak J. Phys. Chem. B **115**, 7218 (2011).

[4] R. P. Sear, S.-W. Chung, G. Markovich, W. M. Gelbart, and J. R. Heath, Phys. Rev. E **59** R6255 (1999); R. P. Sear and W. M. Gelbart, J. Chem. Phys. **110**, 4582 (1999).

[5] D. Pini, G. Jialin, A. Parola, and L. Reatto, Chem. Phys. Lett. **327**, 209 (2000).

[6] A. Imperio and L. Reatto, J. Phys.: Condens. Matter **16**, S3769 (2004); J. Chem. Phys. **124**, 164712 (2006).

[7] A. J. Archer and N. B. Wilding, Phys. Rev. E **76**, 031501 (2007).

[8] A. J. Archer, D. Pini, R. Evans, and L. Reatto, J. Chem. Phys. **126**, 014104 (2007).

[9] A. J. Archer, C. Ionescu, D. Pini, and L. Reatto, J. Phys.: Condens. Matter **20**, 415106 (2008).

[10] A. J. Archer, Phys. Rev. E **78**, 031402 (2008); B. Chacko, C. Chalmers, and A. J. Archer, J. Chem. Phys. **143**, 244904 (2015).

[11] A. Ciach, Phys. Rev. E **78**, 061505 (2008).

[12] H. Shin, G. M. Grason, and C. D. Santangelo, Soft Matter **5**, 3629 (2009).

[13] A. Ciach and W. T. Góźdź, Condensed Matter Phys. **13**, 23603 (2010).

[14] A. Ciach, J. Pekalski, and W. T. Góźdź, Soft Matter **9**, 6301 (2013).

[15] K. von Konigslow, E. D. Cardenas-Mendez, R. B. Thompson, and K. Ø. Rasmussen, J. Phys.: Condens. Matter **25**, 325101 (2013).

[16] Y. Zhuang, K. Zhang, and P. Charbonneau, Phys. Rev. Lett. **116**, 098301 (2016).

[17] Y. Zhuang and P. Charbonneau, J. Phys. Chem. B **120**, 7775 (2016).

[18] M. Edelmann and R. Roth, Phys. Rev. E **93**, 062146 (2016).

[19] D. Pini and A. Parola, Soft Matter **13**, 9259 (2017).

[20] A. Ciach, arXiv:1803.07800v1 (2018).

[21] B. M. Mladek, P. Charbonneau, C. N. Likos, D. Frenkel, and G. Kahl, J. Phys.: Condens. Matter **20**, 494245 (2008).

[22] C. N. Likos, A. Lang, M. Watzlawek, and H. Löwen, Phys. Rev. E **63**, 031206 (2001).

[23] L. Leibler, Macromolecules **13**, 1602 (1980).

[24] M. W. Matsen and F. S. Bates, Macromolecules **29**, 1091 (1996); M. W. Matsen, J. Phys.: Condens. Matter **14**, R21 (2002).

[25] M. A. Glaser, G. M. Grason, R. D. Kamien, A. Košmrlj, C. D. Santangelo, and P. Ziherl, EPL **78**, 46004 (2007).

[26] A. Košmrlj, G. J. Pauschenwein, G. Kahl, and P. Ziherl, J. Phys. Chem. B **115**, 7206 (2011).

[27] See for instance J.-P. Hansen and I. R. McDonald, Theory of Simple Liquids, Academic Press, Oxford, 2013.

[28] M. Tau, A. Parola, D. Pini, and L. Reatto, Phys. Rev. E **52**, 2644 (1995).

[29] K. R. Hall, J. Chem. Phys. **57**, 2252 (1972); I. C. Sanchez and J. S. Lee, J. Phys. Chem. B **113**, 15572 (2009).

[30] V. E. Podneks and L. W. Hamley, JETP Lett. **64**, 617 (1996).